Harmonic Approaches to Non-Intrusive Load Diagnostics
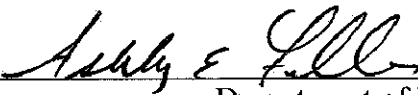
by

Ashley E. Fuller

B.S., Electrical Engineering & Technology (2003), Old Dominion University
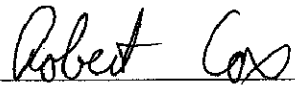
Submitted to the Department of Mechanical Engineering in Partial Fulfillment of the
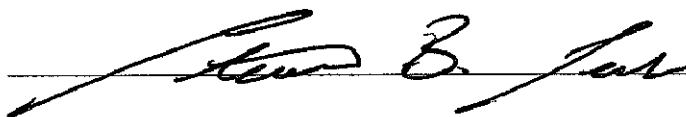Requirements for the Degrees of

Naval Engineer
and
Master of Science in System Design and Management
at the
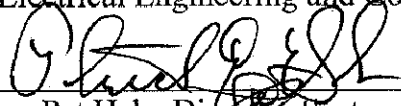Massachusetts Institute of Technology, June 2008

Signature of Author _____
Department of Mechanical Engineering
May 9, 2008

Certified by _____
Robert W. Cox, Assistant Professor University of North Carolina Charlotte
Department of Electrical and Computer Engineering
Thesis Advisor

Certified by _____
Steven B. Leeb
Professor of Electrical Engineering and Computer Science & Mechanical Engineering
Departments of Electrical Engineering and Computer Science & Mechanical Engineering
Thesis Advisor

Accepted by _____
Pat Hale, Director, System Design and Management Fellows Program
Engineering Systems Division
Thesis Advisor

Accepted by _____
Lallit Anand, Professor of Mechanical Engineering
Chairman, Department Committee on Graduate Students
Department of Mechanical Engineering

1

REPORT DOCUMENTATION PAGE

The public reporting burden for this collection of information is estimated to average 1 hour per response, including the time for reviewing instructions, searching existing data sources, gathering and maintaining the data needed, and completing and reviewing the collection of information. Send comments regarding this burden estimate or any other aspect of this collection of information, including suggestions for reducing the burden, to Department of Defense, Washington Headquarters Services, Directorate for Information Operations and Reports (0704-0188), 1215 Jefferson Davis Highway, Suite 1204, Arlington, VA 22202-4302. Respondents should be aware that notwithstanding any other provision of law, no person shall be subject to any penalty for failing to comply with a collection of information if it does not display a currently valid OMB control number.
PLEASE DO NOT RETURN YOUR FORM TO THE ABOVE ADDRESS.

1. REPORT DATE *(DD-MM-YYYY)*	2. REPORT TYPE	3. DATES COVERED *(From - To)*

4. TITLE AND SUBTITLE

5a. CONTRACT NUMBER

5b. GRANT NUMBER

5c. PROGRAM ELEMENT NUMBER

6. AUTHOR(S)

5d. PROJECT NUMBER

5e. TASK NUMBER

5f. WORK UNIT NUMBER

7. PERFORMING ORGANIZATION NAME(S) AND ADDRESS(ES)

**8. PERFORMING ORGANIZATION
    REPORT NUMBER**

9. SPONSORING/MONITORING AGENCY NAME(S) AND ADDRESS(ES)

10. SPONSOR/MONITOR'S ACRONYM(S)

**11. SPONSOR/MONITOR'S REPORT
     NUMBER(S)**

12. DISTRIBUTION/AVAILABILITY STATEMENT

13. SUPPLEMENTARY NOTES

14. ABSTRACT

15. SUBJECT TERMS

16. SECURITY CLASSIFICATION OF:			17. LIMITATION OF ABSTRACT	18. NUMBER OF PAGES	19a. NAME OF RESPONSIBLE PERSON
a. REPORT	b. ABSTRACT	c. THIS PAGE			19b. TELEPHONE NUMBER *(Include area code)*

INSTRUCTIONS FOR COMPLETING SF 298

1. REPORT DATE. Full publication date, including day, month, if available. Must cite at least the year and be Year 2000 compliant, e.g. 30-06-1998; xx-06-1998; xx-xx-1998.

2. REPORT TYPE. State the type of report, such as final, technical, interim, memorandum, master's thesis, progress, quarterly, research, special, group study, etc.

3. DATES COVERED. Indicate the time during which the work was performed and the report was written, e.g., Jun 1997 - Jun 1998; 1-10 Jun 1996; May - Nov 1998; Nov 1998.

4. TITLE. Enter title and subtitle with volume number and part number, if applicable. On classified documents, enter the title classification in parentheses.

5a. CONTRACT NUMBER. Enter all contract numbers as they appear in the report, e.g. F33615-86-C-5169.

5b. GRANT NUMBER. Enter all grant numbers as they appear in the report, e.g. AFOSR-82-1234.

5c. PROGRAM ELEMENT NUMBER. Enter all program element numbers as they appear in the report, e.g. 61101A.

5d. PROJECT NUMBER. Enter all project numbers as they appear in the report, e.g. 1F665702D1257; ILIR.

5e. TASK NUMBER. Enter all task numbers as they appear in the report, e.g. 05; RF0330201; T4112.

5f. WORK UNIT NUMBER. Enter all work unit numbers as they appear in the report, e.g. 001; AFAPL30480105.

6. AUTHOR(S). Enter name(s) of person(s) responsible for writing the report, performing the research, or credited with the content of the report. The form of entry is the last name, first name, middle initial, and additional qualifiers separated by commas, e.g. Smith, Richard, J, Jr.

7. PERFORMING ORGANIZATION NAME(S) AND ADDRESS(ES). Self-explanatory.

8. PERFORMING ORGANIZATION REPORT NUMBER. Enter all unique alphanumeric report numbers assigned by the performing organization, e.g. BRL-1234; AFWL-TR-85-4017-Vol-21-PT-2.

9. SPONSORING/MONITORING AGENCY NAME(S) AND ADDRESS(ES). Enter the name and address of the organization(s) financially responsible for and monitoring the work.

10. SPONSOR/MONITOR'S ACRONYM(S). Enter, if available, e.g. BRL, ARDEC, NADC.

11. SPONSOR/MONITOR'S REPORT NUMBER(S). Enter report number as assigned by the sponsoring/ monitoring agency, if available, e.g. BRL-TR-829; -215.

12. DISTRIBUTION/AVAILABILITY STATEMENT. Use agency-mandated availability statements to indicate the public availability or distribution limitations of the report. If additional limitations/ restrictions or special markings are indicated, follow agency authorization procedures, e.g. RD/FRD, PROPIN, ITAR, etc. Include copyright information.

13. SUPPLEMENTARY NOTES. Enter information not included elsewhere such as: prepared in cooperation with; translation of; report supersedes; old edition number, etc.

14. ABSTRACT. A brief (approximately 200 words) factual summary of the most significant information.

15. SUBJECT TERMS. Key words or phrases identifying major concepts in the report.

16. SECURITY CLASSIFICATION. Enter security classification in accordance with security classification regulations, e.g. U, C, S, etc. If this form contains classified information, stamp classification level on the top and bottom of this page.

17. LIMITATION OF ABSTRACT. This block must be completed to assign a distribution limitation to the abstract. Enter UU (Unclassified Unlimited) or SAR (Same as Report). An entry in this block is necessary if the abstract is to be limited.

Page Intentionally Left Blank

Harmonic Approaches to Non-Intrusive Load Diagnostics

by

Ashley E. Fuller

Submitted to the Department of Mechanical Engineering on May 9, 2008 in Partial Fulfillment
of the Requirements for the Degrees of

Naval Engineer
and
Master of Science in System Design and Management

Abstract

The Non-Intrusive Load Monitor (NILM) is a system that monitors, records and processes voltage and current measurements to establish the operating characteristics of individual loads on a load center from a single aggregate measurement. The NILM can also be used to actively monitor degradation or diagnose specific system failures. Current NILM research conducted at the Massachusetts Institute of Technology's Laboratory for Electromagnetic and Electronic Systems (LEES) is exploring the application and expansion of NILM technology for the use of monitoring a myriad of electromechanical loads. This thesis presents a fundamental guide to understanding NILM operation using laboratory bench testing and demonstrates its potential to detect an array of electric machine failures before they become catastrophic. The NILM's ability to the monitor the current spectrum of electric machines can be used to immediately diagnose multiple common system casualties and detect unusual system operation. Clean current spectrum regions can be exploited by selecting induction machine design characteristics that result in eccentric modulation frequencies occurring in areas free of supply frequency harmonics.
.
Current spectrum analysis was used to demonstrate the NILM's potential to monitor multiple machines from an aggregate source and discuss intersystem impedances. It can be shown that multiple machines with slightly varied physical characteristics, such as induction motor rotor slots, coupled with using clean current spectral regions support automated diagnostic system development. Measurements and experimentation were conducted in the LEES laboratory and the Industrial Support Center electric shop, Boston.

Thesis Advisor: Steven B. Leeb
Title: Professor of Electrical Engineering and Computer Science

Thesis Advisor: Robert W. Cox
Title: Assistant Professor of Electrical and Computer Engineering, UNC Charlotte

Thesis Advisor: Pat Hale
Title: Director, System Design and Management

Acknowledgements

The author would like to acknowledge the following organizations and individuals for their assistance. Without them this thesis would not have been possible.

Table of Contents

List of Figures

List of Tables

1 Introduction

1.1   Background

In theory, the Non-Intrusive Load Monitor or NILM can determine the operating schedule of electrical loads in a target system from measurements made at a centralized location, such as the electric utility service entry [1]. It has shown the ability to identify the operation of specific electromechanical devices in an expanding collection of distribution networks. This thesis establishes a bench test to observe NILM operation using standard test equipment. Voltage and Current are simulated in order to provide a known NILM input and to confirm the output at select stages of NILM data processing.

An induction machine is used to test the NILM's ability to observe common induction machine problems. A framework similar to that used in vibration analysis is employed to locate and explain physical eccentricities associated with common induction machine faults. Initially, both the vibration spectrum and current spectrum are presented in parallel to validate results. Realistic faults are inserted into a test motor, then current and vibration harmonics associated with those faults are confirmed. This thesis identifies specific current spectrum harmonics and uses them to present a potential diagnostic framework.

Current harmonics associated with the physical design of an induction machine present the potential to differentiate multiple motors from an aggregate source. Multiple motors were monitored using a single sensor. A fault was inserted into one machine with the goal of defining a diagnostic scheme that could determine the faulty machine from an aggregate current measurement. The single machine diagnostic framework is then expanded to include a multiple motor framework.

Lastly, the NILM architecture is analyzed using techniques introduced in System Design and Management courses. A new architecture is presented using fewer sub-assemblies and increased capability. The new NILM architecture is constructed, installed aboard a United States Coast Guard Cutter and tested with an improved software package.

1.2   NILM Overview

Figure 1-1 shows the block diagram of a standard NILM. Note that the NILM measures the aggregate current flowing to a bank of electrical loads. It then disaggregates the operating schedule of individual loads using signal-processing techniques [2]. In an engineering plant, the candidate installation locations include generator output busses and distribution panels.
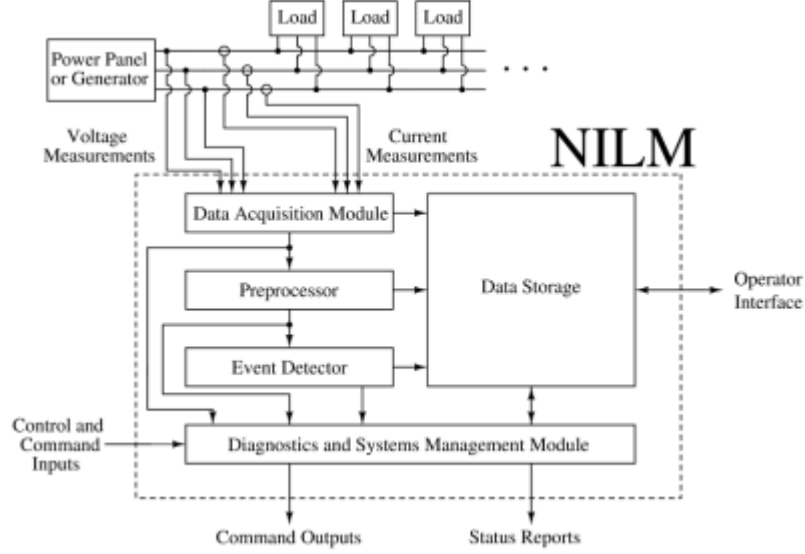
Figure 1-1: Diagram showing the fundamental signal flow path in a NILM

Using measurements of the line voltage and aggregate current, a software-based preprocessor onboard the NILM computes time-varying estimates of the frequency content of the measured line current [3]. Formally, these time-varying estimates, or spectral envelopes, are defined as the quantities [4];

$$a_m(t) = \frac{2}{T} \int_{t-T}^{t} i(\tau) \sin(m\omega\tau) d\tau \tag{1-1}$$

$$b_m(t) = \frac{2}{T} \int_{t-T}^{t} i(\tau) \cos(m\omega\tau) d\tau . \tag{1-2}$$

These equations are essentially time varying Fourier-series analysis equations evaluated over a moving window of length T [5]. The coefficients $a_m(t)$ and $b_m(t)$ contain time-local information about the frequency content of $i(t)$. Provided that the basis terms $\sin(m\omega t)$ and $\cos(m\omega t)$ are synchronized to the line voltage, the spectral envelope coefficients have a useful physical interpretation as real, reactive, and harmonic content [6].

The spectral envelopes computed by the preprocessor are passed to an event detector that identifies the operation of each of the major loads on the monitored electrical service. In a modern NILM, identification is performed using both transient and steady-state information [7]. Field studies have demonstrated that transient details are particularly powerful because the transient electrical behavior of a particular load is strongly influenced by the physical task that is performed [8]. As shown in Fig. 1-2, the physical differences between an incandescent lamp and an induction machine result in different transient patterns. Figure 1-3 demonstrates the positive identification of an induction motor driving a small vacuum pump. Further details of the

11

detection and identification process can be found in Lee [7] and Leeb [6].
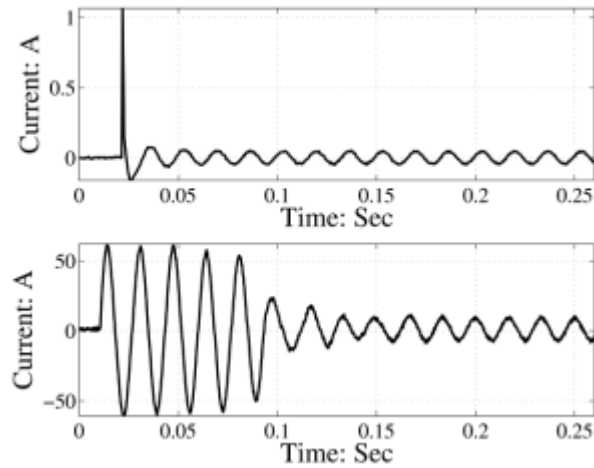
Figure 1-2: Top trace: Current drawn during the start of an incandescent lamp. Bottom trace: Stator current drawn during the start of an unloaded, fractional horsepower induction machine [2].
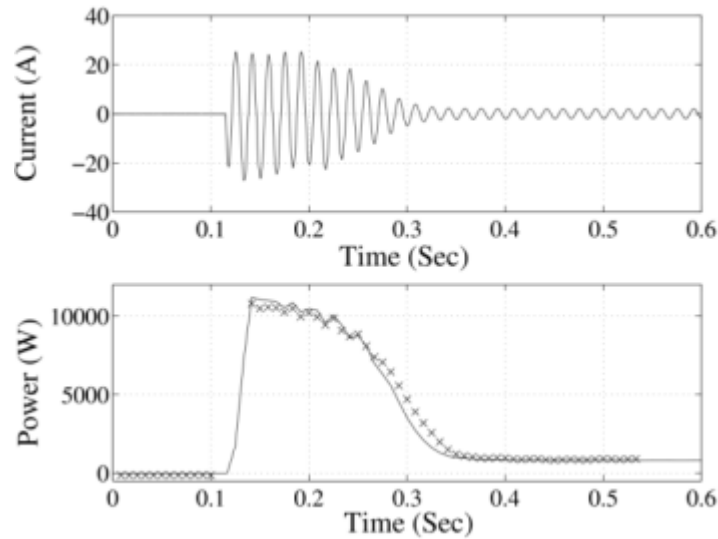
Figure 1-3. Measured current and computed power during the start of 1.7hp vacuum pump motor. Also shown in the power plot is a section of the template that has been successfully matched to the observed transient behavior by the NILM's event detector [2].

The final block in Fig. 1-1 is the NILM's diagnostics and systems management module. This software unit assesses load status using any required combination of current data, voltage data, spectral envelopes, and load operating schedules [9]. The successful application of this module has been demonstrated in numerous publications eg., [3], [7], [8], [10]. Shipboard applications are highlighted in [8], [11], [12], and [13].

As shown in Fig. 1-1, the NILM is designed to interact with human or automated devices in a number of different ways. For instance, the NILM can use its diagnostic information to command certain loads to either commence or cease operations. Additionally, the NILM can provide regular status reports to human operators. To assist in future maintenance operations, the NILM stores all of the relevant data streams (i.e. currents, voltages, operating schedules, etc.) in either a local or remote database [14]. The NILM's storage capabilities make it possible for the operator to perform historical data trending. Note that this off-line analysis can be conducted on a remote PC using convenient software packages such as Microsoft Excel [14]. The following sections describe how these capabilities can be used to prevent or detect certain critical shipboard faults.

1.3 Objectives and Motivation

The NILM is progressing toward production and commercialization to be used in both shipboard and commercial applications. However, there are several important system confirmation tests that should be performed. The NILM must be field tested in systems where diagnostics have already been developed and confirmed. One example of an existing system test that can be used to confirm NILM employment is vibration analysis, which is a part of the Coast Guard's Condition Based Maintenance program. The United States Coast Guard is currently using vibration analysis to monitor the health of shipboard systems to determine system maintenance schedules. There are a number of shortfalls to this system. First, it requires someone familiar with the vibration monitoring process and appropriate training to travel to the ship, configure the target system for analysis, run the test (usually more than once), record the data, and return to enter the data in the appropriate data base, which at the present moment is an Excel spreadsheet.

The vision of the NILM is that a minimal number of sensors will eventually be used to monitor multiple loads. The NILM's ability to monitor multiple loads using an aggregate current measurement must be tested. Current versions of the NILM identify loads simply by looking at transient patterns and steady-state power changes. This may not be enough when looking at multiple systems. One option that will be investigated is the use of system spectral information. Analogous to the mechanical vibration monitoring, the electrical spectral information presents a greater potential for multi-system remote monitoring and overall cost savings.

This thesis will explain the basic operation of each NILM system through a discussion of the internal signal processing and using laboratory bench test examples. A multi-channel waveform generator and signal generator are used to modulate a signal representing current. That current signal is fed into the NILM and each step of signal processing is illustrated. It will assist in the field-validation study by comparing NILM with the current accepted practice of vibration analysis. Common areas of vibration analysis success, such as induction machine imbalance and bearing failure, will be used to confirm NILM results. Induction machine spectral effects will be used to take a detailed look at machine health. This thesis will catalogue and explain common expected spectral effects and use them to show the NILM's superior potential. A procedure for monitoring multiple induction machine loads will be explained and feasibility investigated using the methods established in the single machine diagnostic section. The second

half of this thesis will analyze the current NILM architecture, define the next generation NILM architecture and present this new architecture. The NILM system architecture will be analyzed using OPM (Object-Process Methodology), system decomposition, and subsystem interdependency analysis tools like DSM (Design Structure Matrices) presented in System Design and Management curriculum. The next generation NILM will be constructed according to the output of previously mentioned tools and explained. Lastly, a system (NILM) to system (host or target) interface will be examined to determine a better installation methodology.

.

2 Using the NILM to Monitor Spectral Quantities

2.1 Introduction

The NILM is a monitoring system for extracting useful information about any target or host system that uses electromechanical devices. It has a low installation cost and high reliability because it uses a bare minimum of sensors. One important feature of the NILM is its ability to detect the influence of mechanical effects on electromagnetic actuators like motors. Induction-motor stator currents, for instance, contain a wealth of information about the motor's mechanical load and its operational status [15], [16]. Mechanical non-idealities such as load imbalances and rotor eccentricity cause periodic variations in the amplitude of the current. Such variations can be analyzed either by directly evaluating the frequency spectrum of the current or by examining the spectrum of a demodulated signal. Both analytical approaches are valuable because many important failures can be detected by analyzing current waveforms.

2.1.1 *Current Spectrum Content in Induction Machines*

The dynamics in electromechanical systems can often be seen in the frequency spectrum of electrical current. For example, mechanical vibrations in induction machines can be associated with variations in the physical air gap of the motor [18]. These effects cause a slow variation in the torque produced by the machine, and thus induce a corresponding variation in the amplitude of its current. In effect, the current is said to be amplitude-modulated. The detection of such modulation can be extremely useful from a diagnostic perspective.

Raw current data obtained by the NILM can be analyzed to search for variations such as the amplitude modulation described above. To understand the process of amplitude modulation and its effects, consider the simple system shown in Fig. 2-1. In this system, a general input signal $a(t)$ is fed to a multiplier that mixes it with another signal, $b(t)$.
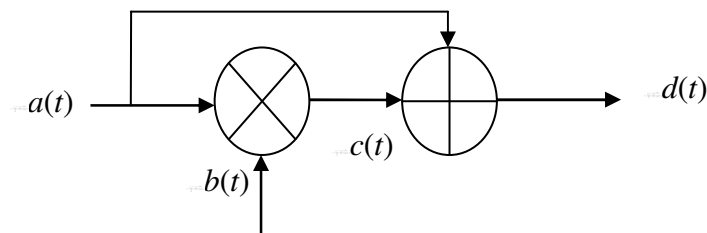
Figure 2-1: Mixer Adder

The sinusoidal signals $a(t)$ and $b(t)$.can be written as Eq. 2-1a and 2-2b,

$$a(t) = A\cos(\omega_A t)$$

(2-1)

$$b(t) = B\cos(\omega_B t + \phi)$$

(2-2)

where A and B are amplitudes, ω_A and ω_B are angular frequencies, and ϕ is a phase angle. The multiplier output, which is denoted as $c(t)$, can be written as:

$$c(t) = \frac{AB}{2}\cos((\omega_A - \omega_B)t - \phi) + \frac{AB}{2}\cos((\omega_A + \omega_B)t + \phi)$$

(2-3)

Following the multiplication process, $a(t)$ is added to the multiplier output, producing the signal,

$$d(t) = \underbrace{A\cos(\omega_A t)}_{1} + \underbrace{\frac{AB}{2}\cos((\omega_A - \omega_B)t - \phi)}_{2} + \underbrace{\frac{AB}{2}\cos((\omega_A + \omega_B)t + \phi)}_{3}$$

(2-4)

Note that the output $d(t)$ is comprised of three components:

1. A carrier signal, a(t).

2. A signal at the difference frequency, $\omega_A - \omega_B$

3. A signal at the sum frequency, $\omega_A + \omega_B$.

In many diagnostic problems, a motor current will take a form similar to the signal $d(t)$. In that case, ω_A would be the line frequency (i.e. 60Hz or 120π rad/sec) and ω_B would be the frequency of some modulating signal. To detect a fault in question, one would search the frequency spectrum for the signals at the sum and difference frequencies.

To demonstrate the effects of amplitude modulation, the system shown in Fig. 2-5 was simulated in Matlab. The two input signals are shown in Fig. 2-2a and 2-2b. The first is a 60Hz input provided as the carrier signal $a(t)$; the latter is a 10Hz waveform provided as the modulating input $b(t)$. The mixer output $c(t)$ is shown in Figure2-2c, and the final output $d(t)$ is shown in Fig. 2-2d. These plots were generated using the constants provided in Table 2-1

Table 2-1: System Inputs

	Amplitude	Frequency	Phase Angle
$a(t)$	1V		
$b(t)$	1V		
ω_A		2π*60Hz	
ω_A		2π*10Hz	
ϕ			0 rads

Fig. 2-3 shows the magnitude of the frequency spectrum of the of the signal $d(t)$ from Fig. 2-6. According to Eq. 2-3, this spectrum should display impulses at the frequencies ω_A, $\omega_{A-\omega_B}$, and $\omega_{A+\omega_B}$. Given the parameter values in Table 2-1, the expected frequencies are 60Hz, 50Hz, and 70Hz, respectively. Given that phi = 0 and A=B, Eq. 2-3 shows that the amplitude of the signals at the sum and difference frequencies are exactly one-half the amplitude of the carrier signal. These predictions match the result shown in Fig. 2-3.
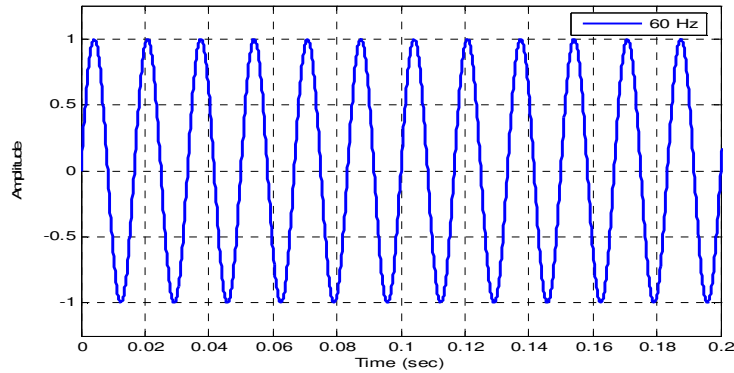
Figure 2-2a: The carrier signal, $a(t)$. In this example, the frequency of this signal is 60Hz.
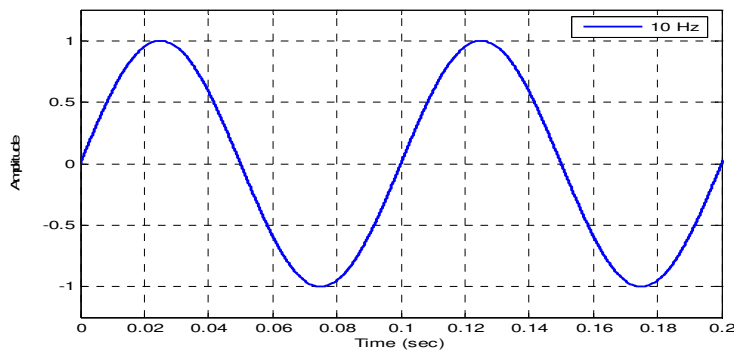
Figure 2-2b: The modulating signal, b(t). In this example, the frequency of this signal is 10Hz.

17
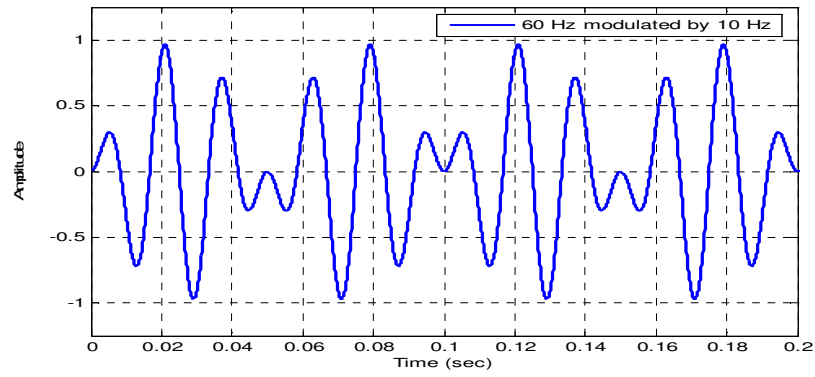
Figure 2-2c: The mixer output, *c*(*t*).
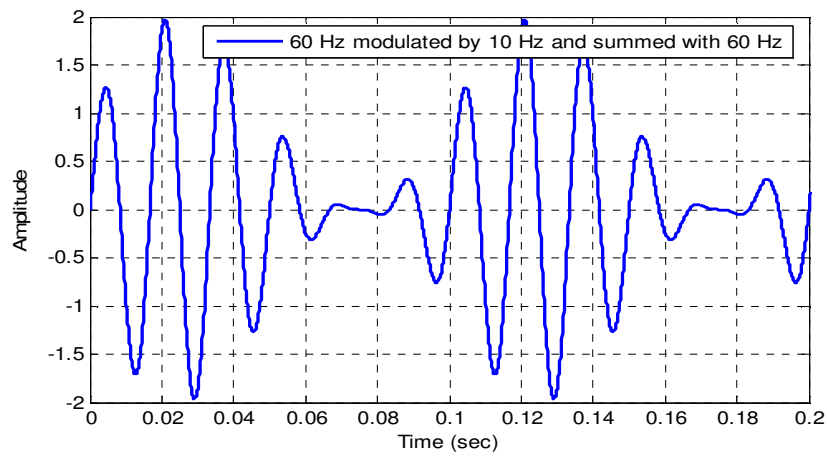
Figure 2-2d: The adder output, *d*(*t*).
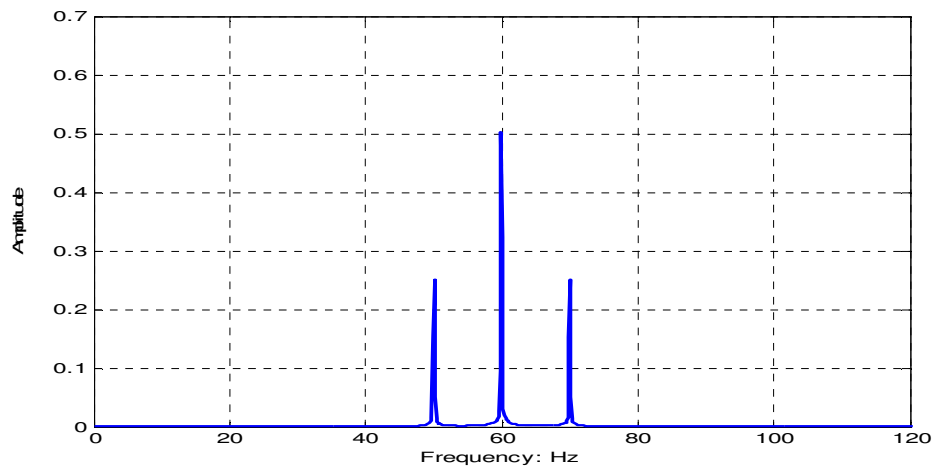
Figure 2-3: FFT of *d*(*t*) from Fig. 2-6d. Note that the amplitude of the sidebands is approximately one-half the amplitude of the 60Hz carrier signal. This is predicted by Eq. 2-3.

2.2 Using MATLAB to produce spectral measurements

There are typically two basic forms of data that can be recorded, stored, and/or displayed by the NILM system. Those two forms are voltage current pairs, sometimes referred to as "raw" and preprocessed data. For this discussion, it is assumed that a single current and voltage measurement is taken using one voltage transducer and one current transducer monitoring a single phase inductive load. It is also assumed that the second generation NILM software and hardware are used, which is discussed in chapter 5 of this thesis. "Raw" data is recorded in a data channel pair, one for measured voltage and one for current. Power is calculated with the pre-processor software, which essentially multiplies the two "raw" channels or voltage and current. Recall that each of these channels for a given dataset can be represented by Eq 2-1 and 2-2. Preprocessed data takes in two channels and produces an even number of channels corresponding to fundamental real and reactive power calculations as shown in figure 2-7. Both "raw" and "preprocessed" data presented in this thesis was generated manually using a simple MATLAB script. This data is presented with an emphasis on useful spectral quantities and minimizes the presentation of non-reactive loads or DC components. Therefore, it is important that the method of both "raw" and "preprocessed" data presentation is explained.

The general Matlab script used to present raw current fast Fourier transforms (FFTs) is presented below in the left column and explained in the right column with examples of the data at significant points on the following page. In this case the "file" is a 60 Hz signal modulated at 10 Hz, which was developed using methods presented later in this chapter.

Code	Explanation

`% For "Bench Test" Test`
`% 60Hz signal amplitude 1 Volt peak – peak`
`% Data taken for 30 seconds`	

`f_samp = 8000;`	Standard sample rate for NILM is 8kHz
`load 'file'`	Load specific files for test
`start = 2000;`	Index where the FFT Starts, use this value to move FFT window through the dataset. Must be $\geq$ 1.
`file_E    = file(:,1);` `file_I     = file(:,2);`	Define each data vector (voltage and Current) (Fig 2-4)
`N_cyc = 200;`	Number of cycles used in the FFT, Influences FFT amplitude.
`f_wall = 60;`	Frequency of Alternating Current.
`N_samp = round((N_cyc/f_wall)*f_samp);`	Normalizes vector length
`ind = (start:start+N_samp-1)';`	Sample pointer initializing at start variable
`file_I_i = file_I(ind);`	Indices (ind) to be represented as vectors (Fig 2-5)
`file_I_i_det = detrend(file_I_i);`	Removes the mean value or linear trend from the specified dataset vector. (Fig 2-6)

hannmeister = hanning(N_samp);	Creates a Hanning window to alleviate spectral leakage. It is important to note that using this function will reduce the amplitude of the FFT by half.
Nfs = 2^16;	Sets the number of points in the FFT
f_x_file = abs(fft(hannmeister.*file_I_i_det, Nfs));	Contains the magnitude of the FFT
fx_x = (0:Nfs/2-1)'*(f_samp/Nfs);	Frequency vector corresponding to the first half of the FFT
plot (fx_x,f_x_file(1:length(fx_x)),'b');	Plotting the resulting FFT (Fig 2-7)
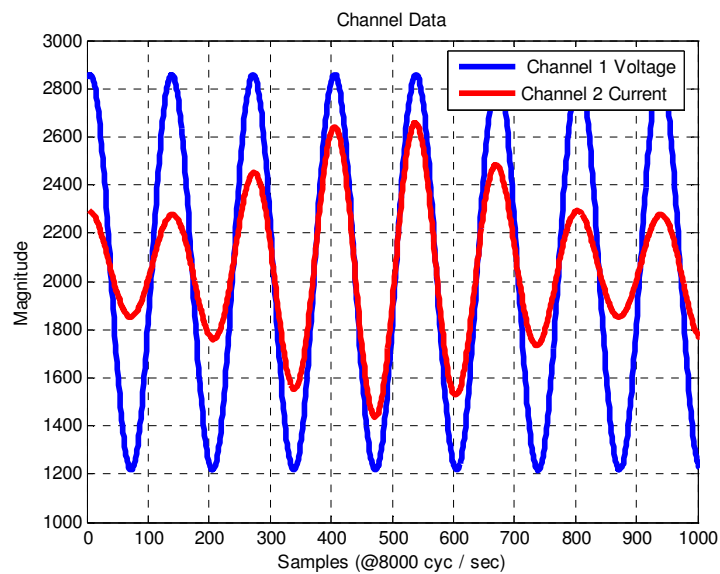
Figure 2-4: Sample Dataset

Dynamic range of the analog to digital device is 4096 amplitude divisions. Thus, data points above 2048 are positive and points below 2048 are negative with 2048 representing zero. Sample dataset presented in figure 2-5 oscillates around an amplitude or "y" value of 2048.

20
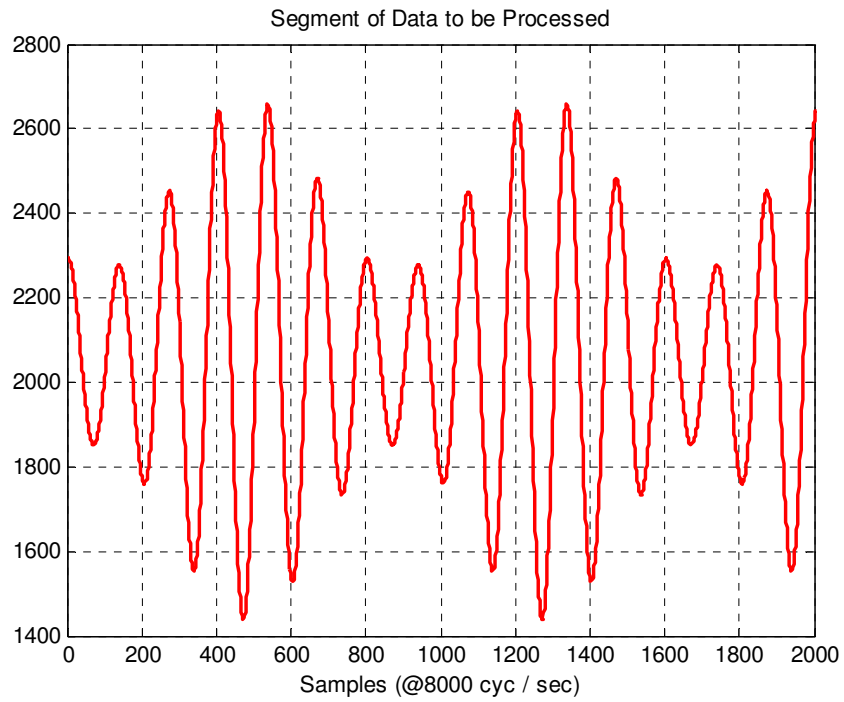
Figure 2-5: Part of Signal used in FFT
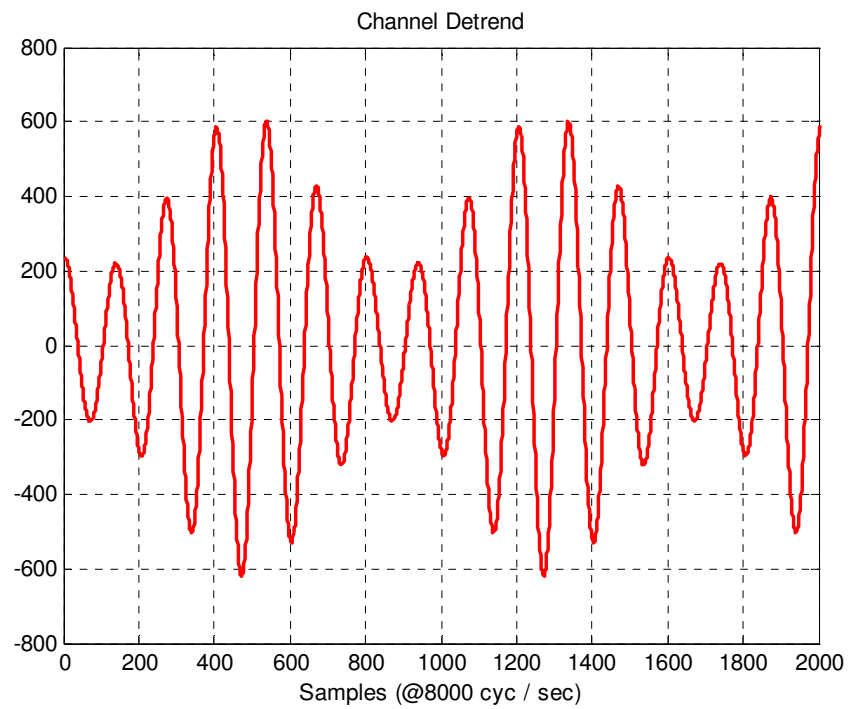
Figure 2-6: Detrending selected dataset

21

FFT of 60Hz Modulated by 10Hz
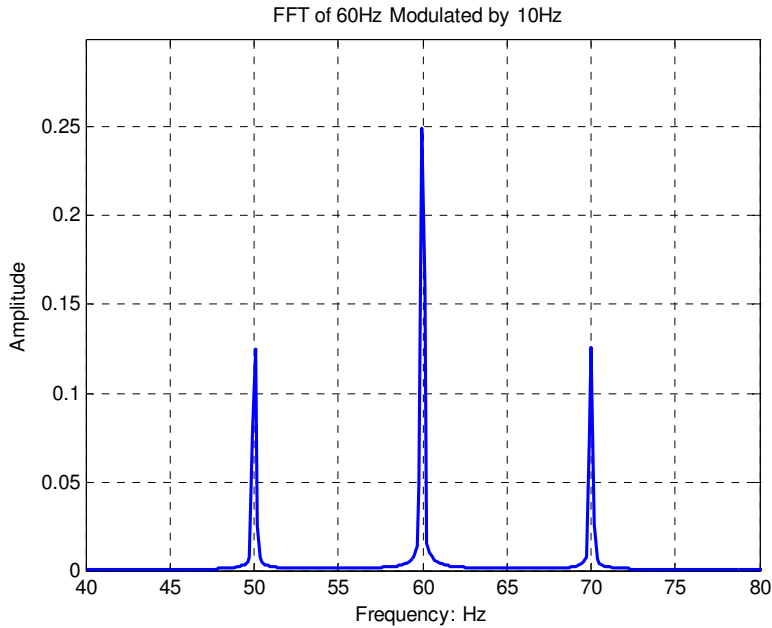
Figure 2-7: Resulting FFT in Matlab

It can be shown that Fig. 2-3 and 2-7 are the same with the exception of the 50 % reduction in amplitude caused by using the Hanning window [19].

2.3   The NILM Preprocessor

The NILM collects and processes two input data streams – line voltage and aggregate current. Using these two quantities, software on the NILM can perform a number of important tasks, including:

- Real-power computation
- Reactive-power computation
- Current-harmonic computation
- Load identification
- Diagnostic analysis
- Power-quality analysis

The first three tasks listed above are performed by the NILM's preprocessor. This software package, which is commonly referred to as "prep," performs a spectral decomposition of the current by computing estimates of the quantities defined in Eq. 1-1 and 1-2. This section proves a qualitative description of the tasks performed by prep, and it also describes how the user should interpret various preprocessed outputs in typical monitoring situations.

2.3.1   *Description of Operation*

Figure 2-8 presents a block diagram of the preprocessor. As shown, prep takes two inputs – line voltage and measured current – and it produces eight outputs. The exact meaning of each output depends on the specific details of a particular installation. Later sections will describe two typical installations.
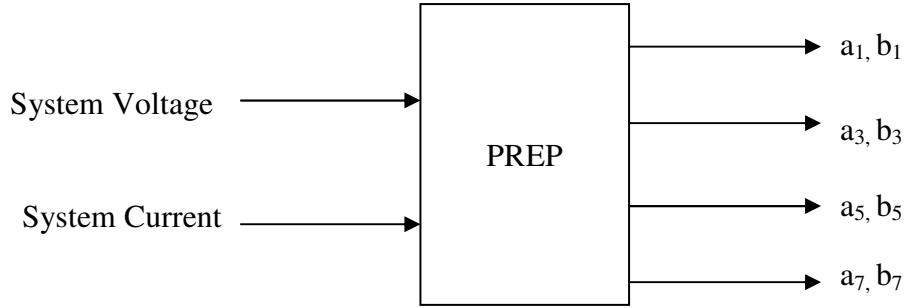
Figure 2-8: Preprocessor Block Diagram

Assuming minimal distortion, the line voltage can be approximated as either a pure cosine or as a pure sine. In this example, it will be assumed that the line voltage is a cosine, Eq. 2-4.

$$v(t) = V \cos(\omega t)$$

(2-5)

In general, the current drawn from such a source will contain a number of harmonics, i.e.

$$i(t) = I_1 \cos(\omega t + \phi_1) + I_2 \cos(2\omega t + \phi_2) + I_3 \cos(3\omega t + \phi_3) + \cdots$$
$$= \sum_k I_k \cos(k\omega t + \phi_k)$$

(2-6)

Equation 2-2 highlights a key fact – the current drawn at any one harmonic frequency is characterized using two quantities, namely an amplitude I_k and a phase shift ϕ_k. The phase shift represents any offset from the line voltage, and the amount of phase shift is strongly dependent on the type of load. Purely resistive devices such as heating elements draw currents that are completely in phase with the voltage, i.e. $\phi_1 = 0$. By comparison, a purely inductive or capacitive load will draw a current that is 90 degrees out-of-phase with the line voltage, i.e. $\phi_1 = \pm 90°$. These loads are often referred to as purely reactive. Many common devices such as motors consist of both resistive and reactive elements. In those cases, the magnitude of the phase shift will lie between 0 degrees and 90 degrees.   The sign of the phase-shift depends on whether the load is either inductive or capacitive in nature.

23

Equation 2-5 suggests that loads draw currents that are rich in harmonics. This general statement reflects the fact that loads can be non-linear. Examples of non-linear loads include devices such as computers, motor controllers, and fluorescent lamps. Typically, these non-linear devices contain a power supply with a rectifier. As an example, Fig. 2-9 presents the current drawn by a small personal computer. As shown, the current is neither a pure sine nor a pure cosine. As predicted by system theory, the current drawn by the device can be represented as a Fourier series of the form presented in Eq. 2-5 [20]. By comparison, the currents drawn by devices such as motors and heating elements draw minimal harmonic content. Thus, these currents can be approximated as:

$$i(t) = I_1 \cos(\omega t + \emptyset_1)$$

(2-7)
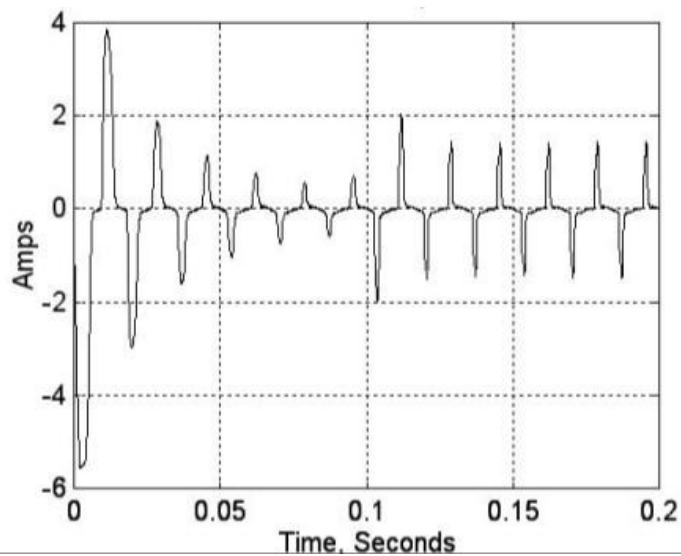
Figure 2-9: Typical Personal Computer Current Measurement [22]
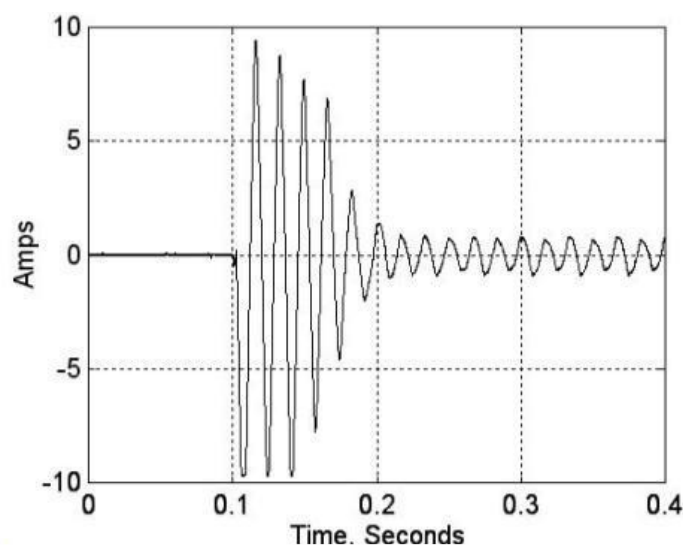
Figure 2-10: Typical Induction Motor Start-up Current Measurement [22]

24

Figure 2-10 shows the current drawn by a typical induction motor. Note that the current can be approximated as a sinusoid with a time-varying amplitude.

It should be noted that the current presented in Eq. 2-5 can be re-arranged through a series of trigonometric manipulations. In effect, the current at each harmonic can be written as the sum of a sine wave and a cosine wave, i.e.

$$i(t) = I_1 \cos(\phi_1)\cos(\omega t) - I_1 \sin(\phi_1)\sin(\omega t) + I_2 \cos(\phi_2)\cos(2\omega t) - I_2 \sin(\phi_2)\sin(2\omega t) + \cdots \quad \text{(2-8)}$$

The cosine at each frequency represents the resistive component of the current and the sine represents the reactive component. Thus, purely resistive devices draw currents containing only cosine terms and purely reactive devices draw currents containing only sine terms. Loads with both resistive and reactive elements draw a combination of both. The representation presented in Eq. 2-7 will be useful in the discussion to follow.

The primary function of the preprocessor is to estimate the real and reactive power drawn from the ideal single-phase source presented in Eq. 2-1. By definition, the real power is

$$P_1 = \frac{1}{T}\int_T V \cos(\omega t) i(t) dt \quad \text{(2-9)}$$

and the reactive power is

$$Q_1 = \frac{1}{T}\int_T V \sin(\omega t) i(t) dt \quad \text{(2-10)}$$

If $i(t)$ is of the form presented in Eq. 2-6, then these results simplify to

$$P_1 = \frac{1}{T}\int_T VI_1 \cos(\phi_1)\cos^2(\omega t) dt = \frac{VI_1 \cos(\phi_1)}{2} \quad \text{(2-11)}$$

and

$$Q_1 = -\frac{1}{T}\int_T VI_1 \sin(\phi_1)\sin^2(\omega t) dt = -\frac{VI_1 \sin(\phi_1)}{2} \quad \text{(2-12)}$$

Similarly, prep also estimates the in-phase and quadrature components of the current at several odd harmonics. At the third harmonic, for instance, it estimates the following two quantities:

$$P_3 = \frac{1}{T}\int_T \cos(3\omega t) i(t) dt = \frac{I_3 \cos\phi_3}{2} \quad \text{(2-13)}$$

25

$$Q_3 = \frac{1}{T}\int_T \sin(3\omega t)i(t)dt = -\frac{I_3 \sin\phi_3}{2}$$

<div align="right">(2-14)</div>

Similar calculations are currently performed at both the 5th and 7th harmonic, although others could be considered if desired.

The complete details of the power calculations performed by the preprocessor are relatively intensive, and they are beyond scope of this thesis [3]. For purposes of illustration, it can be assumed that prep generates a collection of sinusoids internally. As presently implemented [20], the following signals are created:

$$v_{a1} = \cos(\omega t), \; v_{b1} = \sin(\omega t), \; v_{a3} = \cos(3\omega t), \; v_{b3} = \sin(3\omega t),$$
$$v_{a5} = \cos(5\omega t), \; v_{b5} = \sin(5\omega t), \; v_{a7} = \cos(7\omega t), \; v_{b7} = \sin(7\omega t)$$

<div align="right">(2-15)</div>

These phase-locked waveforms are used to estimate the power-related quantities discussed above. For example, the preprocessor uses v_{a1} to estimate the following integral:

$$a_1 = \frac{1}{T}\int_T v_{a1}(t)i(t)dt = \frac{1}{T}\int_T \cos(\omega t)i(t)dt = \frac{I_1 \cos(\phi_1)}{2}$$

<div align="right">(2-16)</div>

This result can be related to P_1 if scaled by the amplitude of the measured line voltage. Similar results hold for the other coefficients.

Because the amplitude and phase of the current change over time, the output of the preprocessor must changes as well. The preprocessor computes the coefficients a_k and b_k over a moving window. This window, which is synchronized to the measured line voltage, is advanced every half-cycle. Thus, new coefficients are produced at twice the line frequency. For a 60Hz service, this implies that power estimates are produced at 120Hz.

After being calculated by the preprocessor, the coefficients a_1 and b_1 can be scaled by the amplitude of the line voltage in order to produce estimates of P_1 and Q_1. These values will vary slowly over time and can be used for identification purposes. Exact details of the computation process are provided in [1].

2.4   Bench Testing

The first step in the process in confirming the NILM is capable of detecting faults that other vibration analysis and current measurement analysis (CMA) techniques can is to present the NILM with a realistic known input and compare the output with the predicted output. Figure 2-11 illustrates the conceptual approach to developing this test.
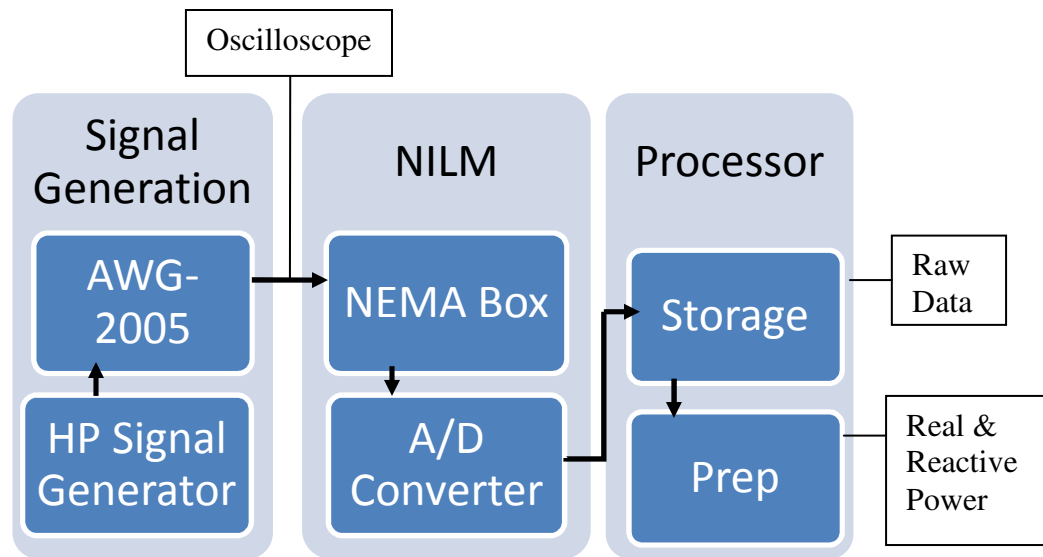
Figure 2-11:   Block diagram of Fundamental Test

2.5   Test Signal Generation

For this test setup, the Tektronix AWG2005 arbitrary waveform generator was used to generate two waveforms representing current and voltage. CMA reveals that a multitude of mechanical modes in induction machines can be monitored. Nearly every electromechanical system has at least one significant mode. Items such as belts, fans, impellors, and pumps exhibit modes that can be monitored in a demodulated current spectrum at a frequency representative of the physical system. To create a test that emulates the simplest scenario for an electromechanical system a 60Hz waveform, representing supply voltage and an Amplitude Modulated (AM) waveform representing current with a single mechanical mode was created. A sample rate of 60 kHz was used to generate each of these waveforms. In order to generate the AM waveform, the AWG2005 requires a separate input to modulate the base frequency (60 Hz in this case). A Hewlet Packard 8656B signal generator was used as the modulating input to the AWG2005. AWG2005. Two channels of the AWG2005 and an oscilloscope were used to ensure proper amplitude, frequency, and phase was entering the NILM box. Figure 2-12 on the following page presents the test setup described above in LEES.
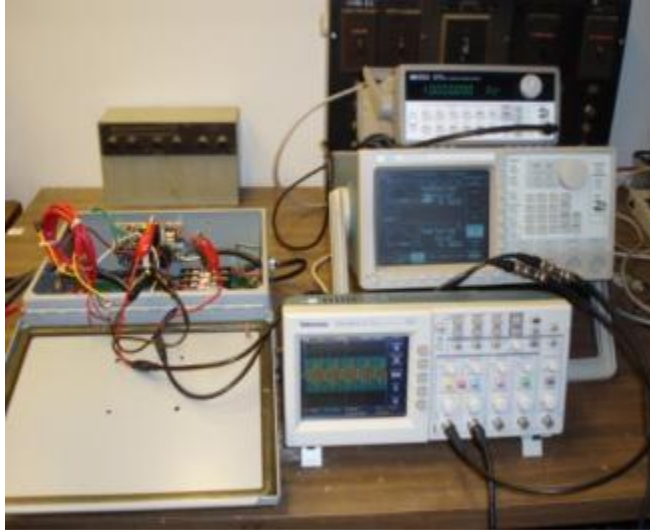
Figure 2-12: "Bench Test" setup
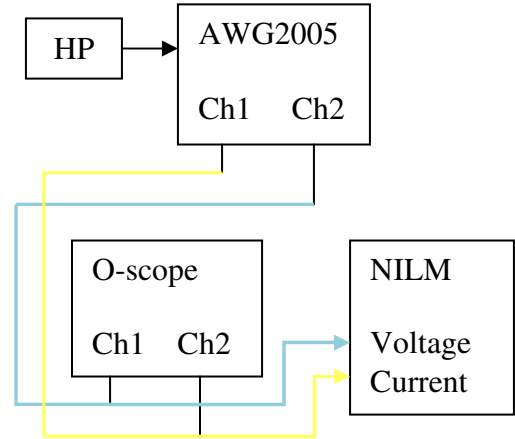
Channel 1 of the Tek AWG2005 is the only channel that can be modulated. Therefore the simulated current originates here but enters channel 2 of the Oscilloscope. This was done because the voltage will be the reference for current phase shifting. Therefore, this set-up will make phase adjustments more straightforward in subsequent test.

In initial NILM installations, sensors are connected directly up stream of the load and tailored to that specific load. The voltage sensor selected in most application is the LV 25-P manufactured by LEM. The current sensor selection requires a closer look at both the transient current signatures as well as typical steady state current ranges within expected load variations. Usually, a current sensor is selected based on the maximum expected current spike of a particular load. The sensor is then scaled as a function of NILM gain, selected current transducer (CT) conversion ratio and measuring resistor(s). In general, current transducers are ideal current sources. The magnetic flux created by the primary current is balanced by a complementary flux produced by driving a current through the secondary windings. A hall device and associated electronic circuit are used to generate the secondary (compensating) current that is an exact representation of the primary current. Thus, the single conductor output of the CT represents an ideal current source representation of the current passed through the CT [21].

The simplest NILM installation uses two input channels, one channel to monitor load voltage and one to monitor load current. For this first test, we used two voltage sources, the first representing the voltage CT input and the second voltage source was passed across a 100Ω resistor to develop a current. Figure 2-14 shows a screen capture of the oscilloscope with the first test signal driven to the NILM box. It presents both the "voltage waveform" (in blue green) and the "current waveform" (in yellow). Ideally, this represents an electromechanical system that has one electro mechanical mode. In this case a current modulation frequency of 10 Hz was used. The amplitude of the simulated voltage is 1 volt peak-to-peak and the modulated voltage or "current" is 1 volt peak-to-peak. This was done to provide enough separation that scaling factors in previous studies like the one done by Patrick Bennett [20].

28
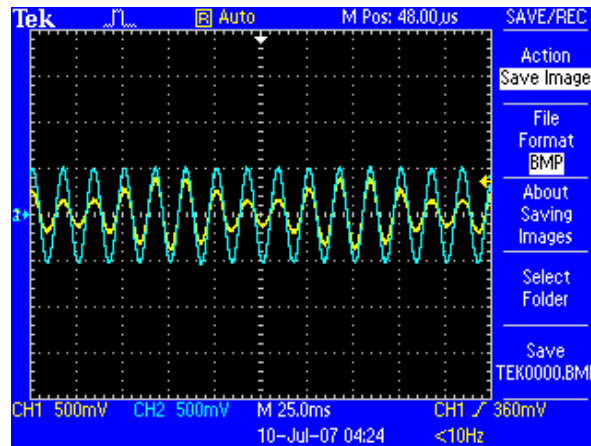
Figure 2-13: Oscilloscope screen capture of both the 60 Hz "voltage" waveform and 60 Hz "current" waveform modulated at 10 Hz in phase
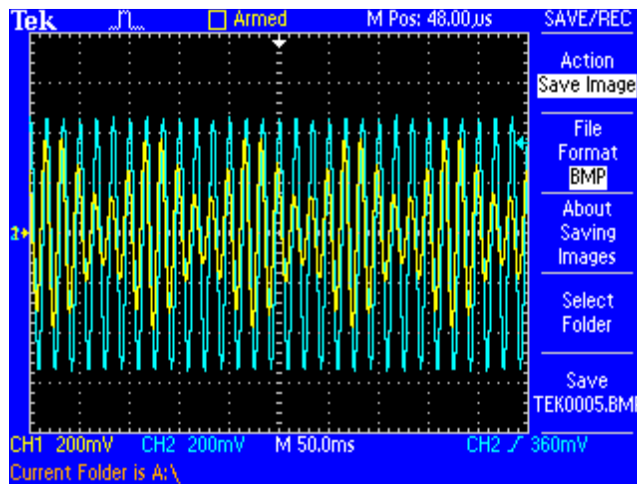
Figure 2-14: Oscilloscope capture of both 60 Hz "voltage" and 60 Hz current" waveform modulated at 10 Hz and leading voltage by 45 degrees

The modulated signal does not appear to quite make 1 V pp in either Fig. 2-13 or 2-14. However, these amplitudes were direct data entries into the AWG2005 user interface; therefore, no effort was made to compensate.

The signals above were fed directly into the terminal block seen in Fig. 2-15 on the following page. The waveforms were relatively small compared to standard shipboard applications to demonstrate the NILM's ability to handle small signals and observe system noise. Figure 2-15 shows the signal entering the NILM input terminal block.

29
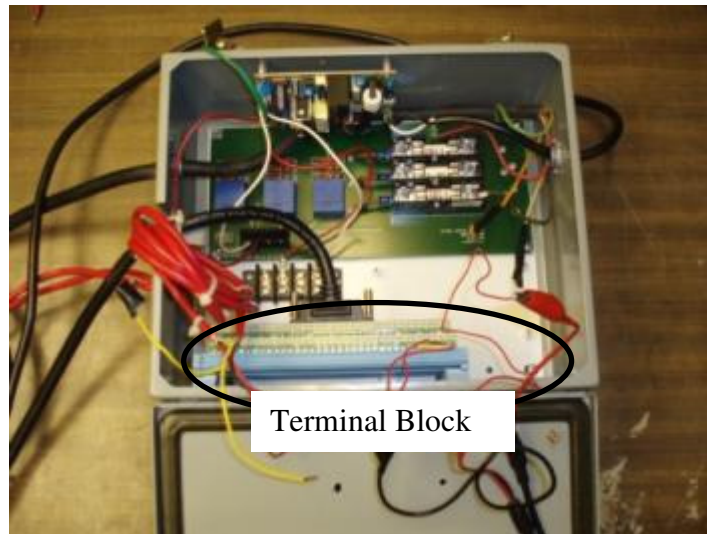
Figure 2-15: Test Signal Generator output to NILM connection

2.6 NILM Configuration and Measurement

The NILM computer was configured similar to standard marine installation with a couple of exceptions. In order to look at the Analog to Digital A/D gain function, the gain code for the voltage channel was set to 1, meaning it would appear to be doubled. The gain code for the current channel was set to zero for a 1-to-1 relationship.   The NILM voltage and current channels were sampled at a rate of 8 kHz for 30 seconds.

2.6.1 *Representing Current*

In order to generate a clean realistic signal, a waveform generator (TEK AWG2005) was used which imposes some minor modeling limitations. Most importantly, the output of the function generator more closely resembles an ideal voltage source whereas the output of the typical LEM current transducer output looks more like an ideal current source. The output of the waveform generator was driven across a resistance inducing a representative current. However, to stay true to the output of the test setup, both channel 1 and 2, representing voltage and "current" respectively, will both be referred to as voltages. Channel 2 instantaneous voltage can be divided by the terminal board resistance to determine NILM current.   This will also be important in representing power.

Both the voltage and current signals were driven into a 100Ω resistor (across the terminal board pins 33 to 67 and 34 to 68 respectively). Comparing figures 2-7 and 2-3, one can see that the NILM has effectively captured the exact input waveform created by the test setup. Referring back to figure 2-13, the agreement between the oscilloscope depiction of the input and figure 2-16 on the following page confirm NILM operation up to the preprocessor.
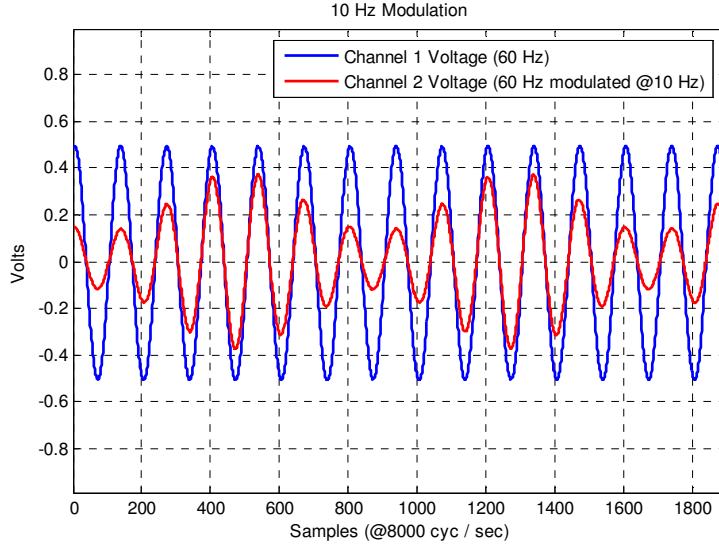
2-16: **Channel Output from the NILM**

In general, the amplitude of the voltage representing a current for such a mixed signal can be calculated by Eq. 2-16 where A is the amplitude of the carrier, M is the amplitude of the modulation, ω_c is frequency of the carrier (in radians), ω_m is the frequency of the modulation (in radians), t is time in seconds and $\emptyset$ is the phase shift between the carrier and modulated signals (in radians).

To confirm that there are no other "hidden" signals in the output waveform a fast Fourier transform (FFT) was performed on the raw data using MATLAB. The FFT should show amplitude consistent with the time domain plot. In general, the amplitude of the voltage representing a current for such a mixed signal can be calculated by Eq. 2-1 where A is the amplitude of the carrier, M is the amplitude of the modulation, ω_c is frequency of the carrier (in radians), ω_m is the frequency of the modulation (in radians), t is time in seconds and φ is the phase shift between the carrier and modulated signals (in radians).

$$V_{out} = A\cos(\omega_c t) + \frac{AM}{2}\left[\left(\cos\left((\omega_c - \omega_m)t\right) + \emptyset\right) + \cos\left(\left((\omega_c + \omega_m)t\right) + \emptyset\right)\right]$$

(2-17)

31

2.6.2 *Power*

The NILM uses measurements of voltage and current to produce estimates of real and reactive power consumption (henceforth referred to as P and Q, respectively). For a single phase system, the NILM is supplied with the voltage from line to neutral and the current flowing to any loads downstream of the monitoring point. Real power (P) is produced by current which is in-phase with voltage and reactive power (Q) is produced by current which is 90 degrees out of phase with voltage. It also estimates the higher harmonic content of current to produce the first three odd harmonics of real and reactive power (referred to as *Pk* and *Qk* for the *kth* harmonic of P and Q, respectively). If the same sinusoidal voltage is applied to a resistor, capacitor, and inductor, the *NILM* would produce positive P with zero Q for the resistor, positive Q with zero P for the inductor, and negative Q with zero P for the capacitor. The convention of using a power angle measured in the clockwise direction from the real axis is employed, so that the power angle for an inductor is +90 degrees while the power angle for a capacitor is -90 degrees [17]. For a more in--depth description of the NILM calculations used to determine P and Q, see [20].

The NILM was given one signal pair from the waveform generator. Table 2-1 below lists the variables for each test. All test used 60 Hz as the principle frequency. Channel 2 was chosen to lead channel 1 simply because current generally leads voltage in predominantly inductive circuits. These tests were run and preprocessed data recorded for each.

Table 2-2: Phasor Test

Test	Modulation (in Hz)	Phase shift (in degrees)
1	10	0
2	10	45
3	20	0
4	20	45
5	30	0
6	30	45

In order to check the preprocessor or prep software, the initial input waveform depicted in Fig. 2-7 was used. Data from test number 1 (60 Hz voltage channel and the 10 Hz modulated current channel) was used and NILM outputs were plotted in the Fig. 2-18 and 2-19 below.

The fact that this test used an ideal voltage source to develop a current across a resistance becomes very important in looking at representative Power. For this reason, we will scale power to an average value of 1. Because the amplitudes can always be scaled, the goal of the specific test was not to demonstrate amplitude accuracy but to show that frequency and phase response were accurate. However, the amplitude should reflect a value that can be linearly scaled to ensure accuracy over the target spectrum.
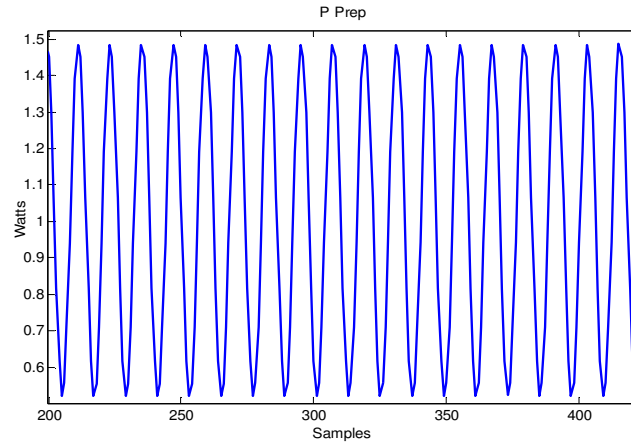
2-17: Preprocessor Output of Real Power
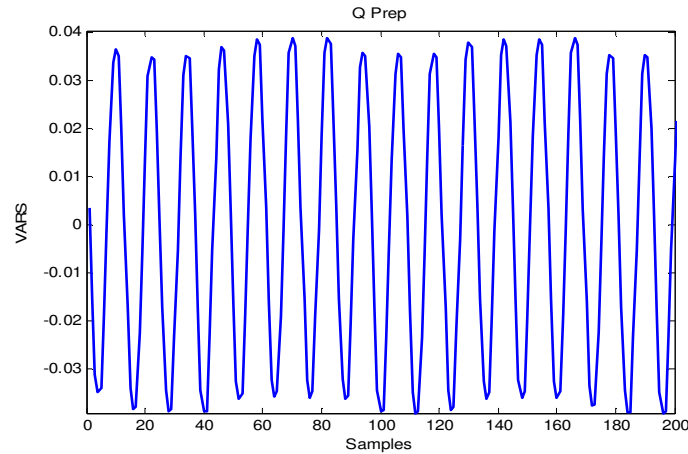
2-18: Preprocessor Output of Reactive Power

Figures 2-17 and 2-18 reflect expected outputs. The real power fluctuates around 1 Watt while reactive power fluctuates around zero. Ideally reactive power would have no fluctuations but some can be seen in above. However, the fluctuations are less than 0.04 VARs which is less than 5% of the average wattage. These minor fluctuations could be caused by preprocessor filtering techniques, internal noise, external noise or a little of all three. Keeping in mind that the input signal amplitudes are extremely small compared to typical values, these fluctuations are negligible.

In order to establish a reference, the expected of a strictly resistive test was used to normalize the remaining section FFT plots to 0 dB = 250mW. This was done by creating a synthetic voltage and current signal using Matlab with a known amplitude and running it through the preprocessor. This established a reference for later test that adjust the phase angle between the voltage and current. One note with regard to the FFTs of power in this section, the same Matlab code presented in the section 2-1 was used to create these FFTs. The cursor feature in the plot function was used to present the amplitude of the key spectral quantities.

33
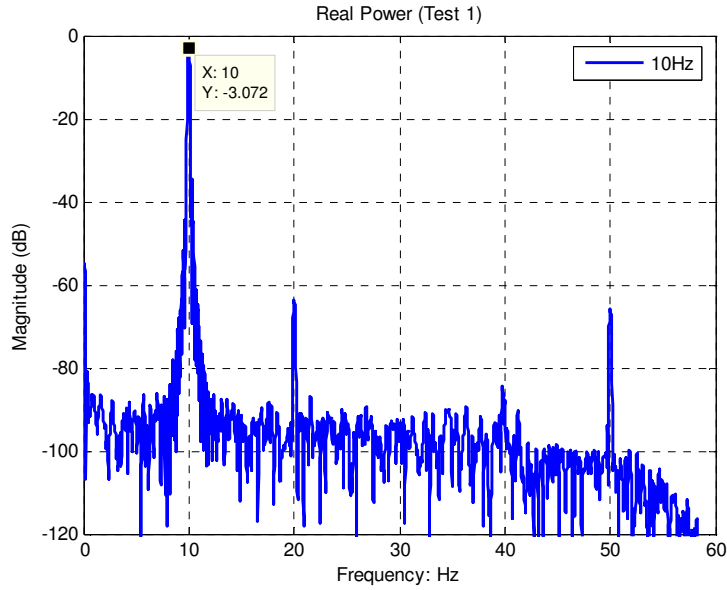
2-19: FFT of Preprocessed Real Power
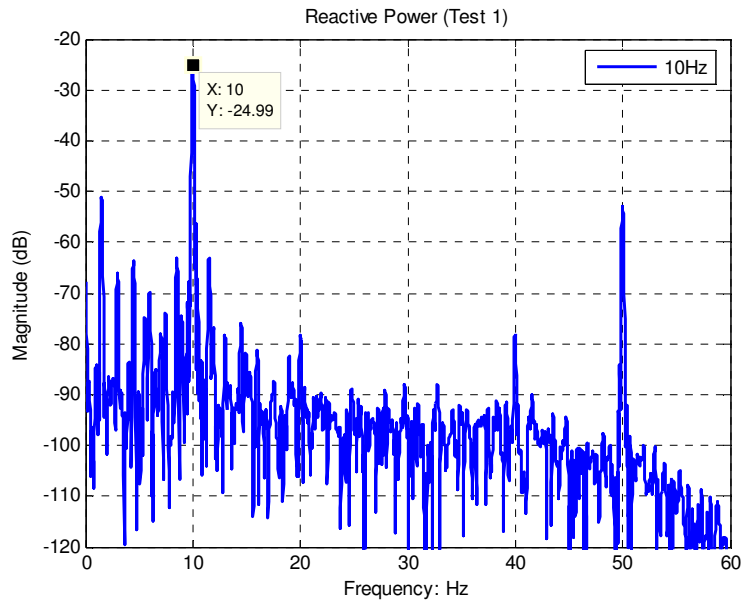
2-20: FFT of Preprocessed Reactive Power

Note the plots in Fig. 2-19 and 2-20 are consistent with corresponding time domain plots on the previous page. There is also another spectral component that exists at 70Hz. However, because of the Nyquist rate, the sampling rate of prep (120 Hz) limits the frequency of the results to 60 Hz so higher spectral quantities due exist but are not displayed without changing the preprocessor.
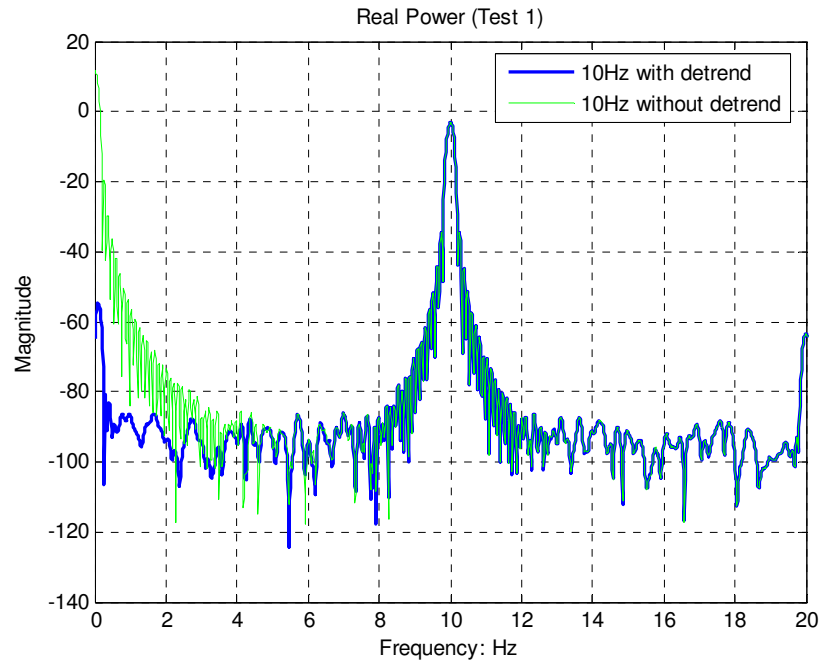
Figure 2-21: Figure 2-21 with plot of 10Hz signal without "detrend" function showing DC component

A close look at the actual DC component reveals an amplitude of +12db. This could be caused by test equipment coupling or preprocessor filtering techniques.

2.6.3 *Applying a 45 degree leading phase shift to "Simulated Current"*

The waveform generator was adjusted to perform the second test. This was done by advancing the phase of the signal being driven into channel two of the NILM by 45 degrees. Figure 2-22 presents the scope display capture of channel one (blue green) and channel two (yellow) fed into the NILM terminal board. The only adjustment made to the test setup in test one was the adjustment of the phase angle between channel one and two (channel two now leads channel one by 45 degrees).
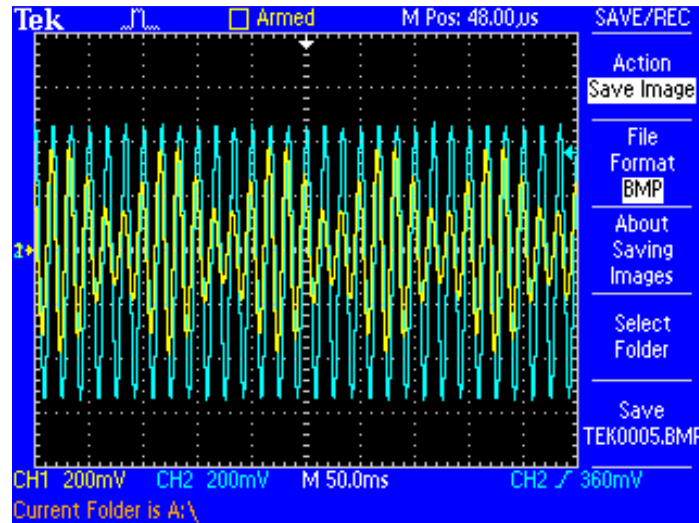
2-22: Oscilloscope capture of 60Hz "voltage" and 60 Hz modulated at 10 Hz "simulated current"
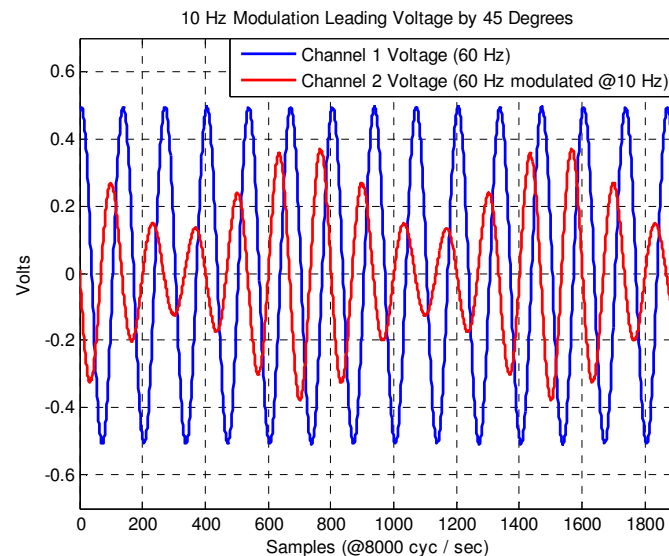
2-23: NILM Measurement Output

As the modulated voltage representing current was shifted, the amplitude appeared to decrease. The FFT of the prepped data will present a better picture of what is actually happening here.

Next, the phase shifted "simulated current" seen in Fig. 2-16 was fed into the preprocessor software. The preprocessor output in Fig. 2-24 and 2-25 (real and reactive power respectively) appear expectedly different.
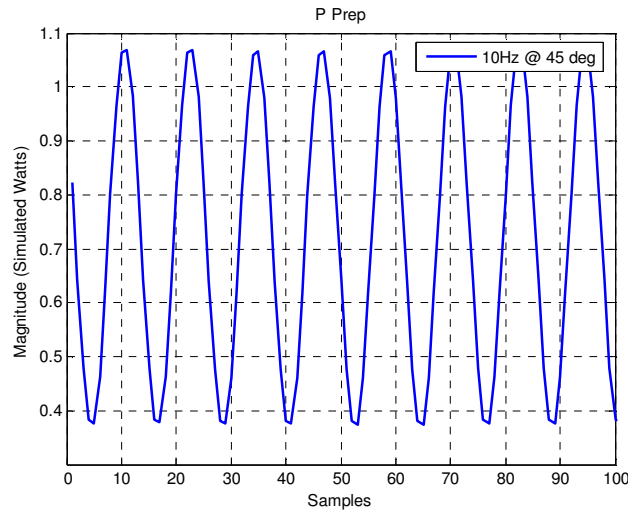
2-24: Preprocessor Output of Real Power (Simulated Current Leads Voltage 45 deg)
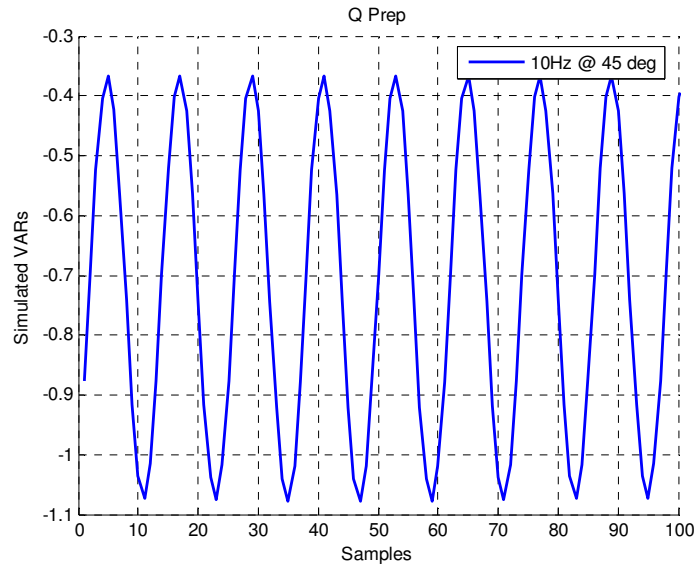
2-25: Preprocessor Output of Reactive Power (Simulated Current Leads Voltage 45 deg)

Observing Fig. 2-24 and 2-25, it appears that the preprocessor software is reflecting the fact that both real and reactive power shows up on a DC level that is equal to $1/\sqrt{2}$, which is what would be expected with a 45 degree shift between voltage and current. A look at the FFTs of real and reactive power should confirm the time domain data.
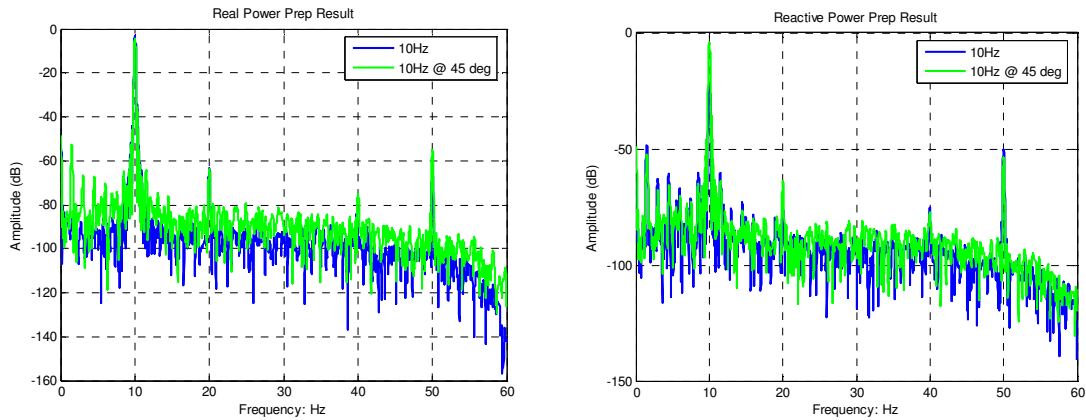
Figure 2-26: Preprocessor Outputs (Channels 1 and 2)

Figures 2-26 is presented simply to show an amplitude plot of the entire preprocessor output. In order to get more value, Fig 2-27 focuses in on areas around 10 Hz.
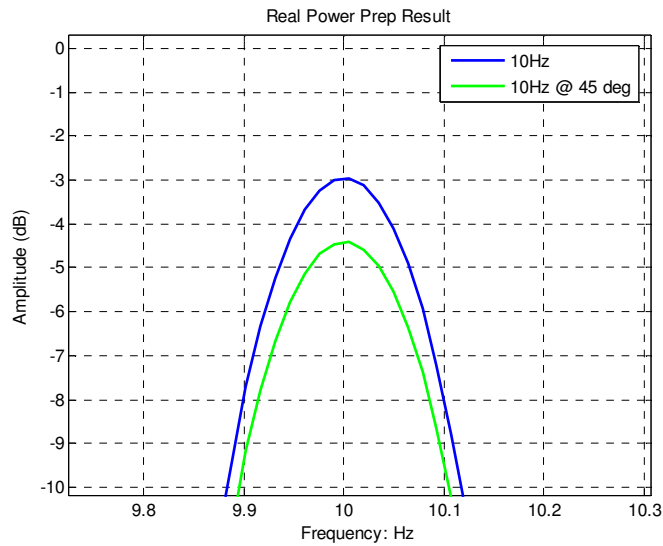
Figure 2-27: Closer look at Preprocessor Real Power

The unshifted 10Hz modulation spectral component shows up at 10Hz and Minus 3 dB. The spectral component shifted 45 degrees shows a 1.5dB reduction in amplitude which again is expected. A 45 degree shift can be shown to reduce the DC level of the spectrum to $1/\sqrt{2}$.
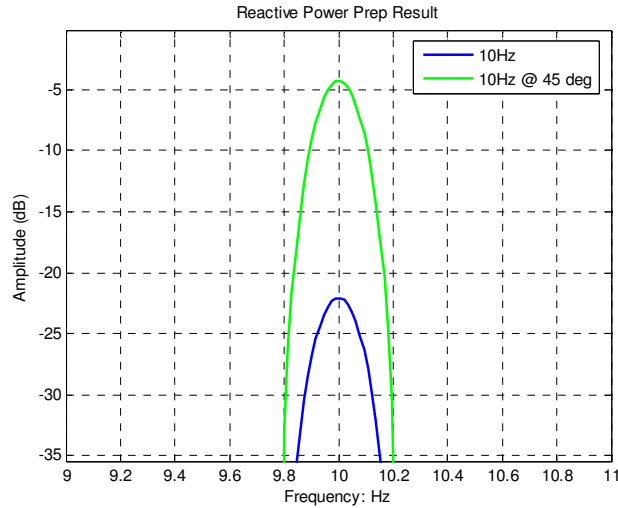
Figure 2-28: Closer look at Preprocessor Reactive Power

There are two interesting things about Fig. 2-28. First is that the reactive power in the phase shifted 10Hz modulated case does in fact show a minus 4.5dB amplitude. And second, the inherent noise of the system can be seen. We know there should be little to no reactive component in the unshifted case. Fig. 2-28 indicates that a component with an amplitude of approximately -23db, which translates to less than a femtowatt. The remaining test provided similar results on all accounts.

2.6.4 *Conclusion*

Electromechanical systems are inherently designed with mechanical resonating modes that can be detected in electrical current signatures. This is one of the fundamental principles the NILM system exploits. The NILM records and processes voltage and current relationships and presents robust data sets, including but not limited to real and reactive power relationships, that can be used to make technical decisions. The tests above sought to use a two channel waveform generator to model the simplest electromechanical relationship, an electromechanical system with a single resonate mode with the goal of observing the NILMs accuracy in data recording, multi-channel phase and amplitude relationships, preprocessor operation and the level of system noise. This simple test confirmed the standard NILM setup operates as designed in each of the observed cases.

3 AC Motor Analysis

3.1 Introduction

The NILM is able to monitor and report on a number of key motor faults. The NILM performs these diagnostics using both the current spectrum and the spectral envelopes discussed previously. The use of the NILM in this capacity is extremely attractive because the NILM itself is installed in a central location and does not require special motor access. Additionally, the NILM offers the opportunity to consider monitoring multiple motors simultaneously.

The next two chapters provide an initial demonstration of the NILM's capabilities as a motor-monitoring device. This chapter begins by examining the use of the NILM to monitor a single motor; Chapter 4 considers the possibility of monitoring multiple motors by applying the process used in this chapter but using an aggregate current signal.

3.2 General Procedure

Using information contained in [24], the most relevant motor-related problems were identified and bulleted on the following page. The two most common problems, motor imbalance and bearing faults, drove the development of specific tests in laboratory. These test involved imposing faults representative of rotor imbalances and bearing faults seen in the field. The ultimate vision of this application is that an aggregate sensor will be used to monitor multiple machines in an automated fashion. This vision shapes the way the NILM is configured to monitor and the procedure used.

Ultimately, the goal is to develop a method to autonomously monitor and report on multiple motors with a single aggregate sensor. With this in mind, it is clear that a method must be established to autonomously monitor and report on a single motor with a single sensor. A process is presented that involves defining physical machine characteristics, monitoring the current spectrum to confirm a machine with defined characteristics can be identified, "locking on" to spectral current components associated with that machine to track speed and / or slip, and using that speed / slip with the corresponding spectral components associated with imbalance or bearing faults to determine machine health.

3.3 Common Motor-Related Problems

The diagnostics discussed in this chapter involve either a spectral decomposition of the current or its spectral envelopes (i.e. P_1 and Q_1 from Chapter 2). In order to develop a NILM diagnostic system to determine the health of motor driven systems, some specific initial target problems should be identified. As a starting point, key faults that were known to affect the current spectrum [15] were investigated; they are listed on the following page.

- An unbalanced rotating element
- Bearing faults
- Misalignment between motor and load
- Bent shafts
- Shaft radial thermal expansion
- Cavitation
- Water hammers
- External vibration

The first two bullets above represent the most commonly documented root causes of motor failure [24]. Initially, a simple single phase axial fan motor were used to establish the NILM's ability to detect evidence of an imbalance and bearing faults.

3.4 Developing NILM-based Diagnostics for Induction Machines

To detect faults such as the ones discussed previously, a NILM monitoring aggregate current flow must follow a systematic procedure consisting of both load identification and subsequent diagnosis. This section describes the process that has been developed during the course of this project. The approach has been used to monitor both single and multiple motor loads. Figure 3-1 shows a block diagram of the proposed monitoring process. Digital stator current data is passed to a signal processing routine, which selects and captures a specific window of time domain data. The fast Fourier transform is generated and the resulting spectral current data is first used to confirm the presence of induction machine loads. For this specific example, motor slot harmonics are identified using key motor parameters entered into a graphical user interface (GUI). This GUI should be similar to the one designed in [23] but would present current diagnostic information. The GUI would have a data entry function where the key motor parameters for the machines under test would be entered. This information would be fed into the Information and Computation function, which stores the key parameters and uses a slot harmonic calculation to determine slip. It then packages this information in a vector and passes it to the diagnostic subroutines according to preferences entered into the GUI.
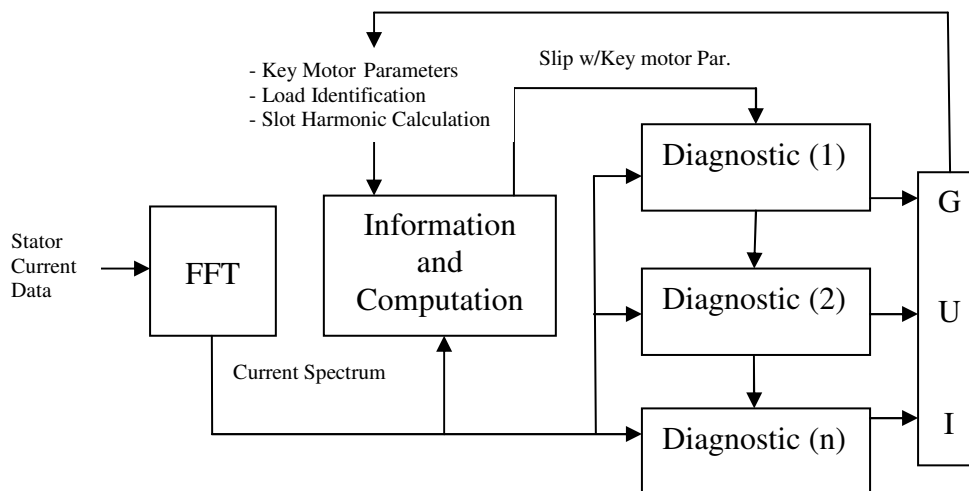
Figure 3-1: General Single Motor Diagnostic Process Block Diagram

41

The diagnostic modules are arranged in a hierarchy associated with the needs of the end user. The output to each loaded diagnostic is controlled by a graphical user interface based on system requirements. There are some steps in this process that need to be discussed. Those steps are presented in the following sub-section.

3.4.1 *Identify key motor parameters*

The first step, which must be undertaken before monitoring, is to determine certain key motor parameters such as the line frequency, the number of pole pairs, bearing geometry, machine loading, and environment. Most of the machine parameters needed to make initial slip calculations can be found on the machine name plate. Given that ultimately an aggregate sensor will be used to monitor multiple loads, a single system supply frequency can be assumed. In this case, the current spectrum FFT can be used to determine the system supply frequency by looking at the spectral component with the highest amplitude and confirming this using supply harmonics. Additional information required can be obtained from the manufacturer, such as the number of rotor slots, bearing geometry, etc. The complete list of key parameters is based on the type(s) of diagnostics desired.

3.4.2 *Estimate speed*

The second step in the monitoring process is to identify motor speed. This requires a combination of NILM's powerful load-classification routines and the detection of certain key spectral quantities. The NILM's load classifier, which is described in [23], can identify specific loads operating. Once such a decision has been made, the NILM can use the parameters determined previously to estimate the speed of that motor.

A number of sensorless speed estimation procedures have been identified over the years [24]. The estimation procedure used in this thesis relies on the successful identification of several rotor-slot harmonics. Further information about these signals and the speed-estimation procedure are presented in Section 3.4.3. If identical motors are operating, the rotor-slot harmonics could be used to assist in the identification process. More details are presented in chapter 4.

3.4.3 *Verification of Load Identification and Speed Estimate*

Rotor-slot harmonics are not the only speed-related signals present in the current spectrum. One other speed indicator that can be used to verify the speed estimate is eccentricity-related components that appear as modulations of the 60Hz line current. These signals can also be used to detect certain critical faults such as load imbalances. While these spectral components are not as accurate as slot harmonics, they are valuable in the role of confirming the primary speed estimation method.

3.4.4 *Health Monitoring and Fault Detection*

Once motors have been successfully identified, it is possible to start tracking certain key spectral quantities that are indicative of failure. In this thesis, two different types of faults are considered – load imbalances and bearing wear. The first of these can be monitored using the eccentricity-related signals described previously; the latter can be monitored by tracking certain characteristic bearing frequencies that are present in the current spectrum. Further details are presented in Section 2.6.2.3.

3.5 Experimental Verification

The steps in the process described in Section 3.4 were experimentally verified in the laboratory. Initial experiments were performed using a single-phase axial fan motor. The motors in question are ¾ HP machines donated by the Industrial Electric Shop (IES) on the 1st District Coast Guard base in Boston, Massachusetts. These machines were previously used for intake and exhaust ventilation in the main engine room aboard one of the Coast Guard's 49ft buoy boats (Fig. 3-2a). Figure 3-2b shows a photograph of one of the motors, and Table 3-1 summarizes key motor parameters.

Figure 3-2: (a) One of the Coast Guard's 49ft. buoy boats and (b) one of its exhaust fans. The fans used in this thesis are identical to the one pictured.

Table 3-1: Marine Motor Data

Make: Marathon Electric / Marine Duty IEEE			
Model: 4VF 56C34 F5506A		Type: SCS	Design: B
Code: N	Bearings: 6302	Voltage: 120V	Current: 10.8A
RPM: 3450	Single phase	60 Hz	¾ Hp
# Rotor Slots: 34		Poles: 2 (1 pair)	

The following sections describe the experimental verification of each of the key parts of the process described above. The issues relevant to this thesis are:

- Speed estimation using rotor-slot harmonics
- Detection and use of eccentricity-related signals
- Detection and use of characteristic bearing frequencies

3.5.1 *Estimating Speed with Slot Harmonics*

An accurate speed estimate is key to the monitoring process described in this chapter. Speed-related current modulations arise from the interaction of variations in the air-gap permeance with the air-gap magnentomotive force (mmf). Variations in the air-gap permeance are caused by rotor slotting and rotor eccentricity. It can be shown that these effects result in current harmonics at the following frequencies [24]:

$$f_{sh} = f_1 \left[(kR \pm n_d) \left(\frac{1-s}{p} \right) \pm n_w \right] \tag{3-1}$$

In Eq. 3-1, f_1 is the supply frequency, k is an integer in the range $\{0,1,2...\}$; R is the number of rotor slots; $n_d = 0,\pm 1,...$, is the order of rotor eccentricity; s is per unit slip; p is the number of poles pairs; and $n_w = \pm 1, \pm 3,...$, is the air-gap mmf harmonic order [24]. Given values for f_1, R, and p, assuming $k = 1$ and static eccentricity (n_d=0), one can use these slot harmonics to estimate the slip and subsequently the speed from the equation:

$$s = \frac{N_S - N}{N_S} \tag{3-2}$$

where N_S is the synchronous speed[1] of the machine in RPM and N is the actual speed in RPM. Initial testing of the speed estimation process was performed using the test machine described above. The current procedure follows three steps:

1. Determine a range of values for four, low-order rotor-slot harmonics using Eq. 3-1 and n_w in the range between -3 and 3 (low order). An initial slip estimate is also required. In our initial tests this estimation is obtained from direct measurements, but one could also use the rated speed written on the boiler plate.

2. Examine the current spectrum in the range calculated.

3. "Lock on" to the four low order slot harmonic spectral components.

4. Determine speed estimate.

---

[1] Synchronous speed is the number of pole pairs divided by 3600, (N_S = 3600/p).

To demonstrate this process, several experiments were performed using the test motor identified in Table 3-1. In each experiment, the speed of the motor was changed by placing a different weight on one of the fan blades. Table 3-2 lists the values needed to estimate the locations of the four slot harmonics discussed previously. Given an initial speed estimate of approximately 3500RPM, the four slot harmonics are expected to appear in the range between 1800Hz and 2200Hz. This is clearly indicated in Fig. 3-3.

Table 3-2: Slot Harmonic Variables

$F_1 = 60$ Hz	$k = 1$
$R = 34$	$n_d = 0$
$p = 2$	$n_w = \pm1, \pm3$
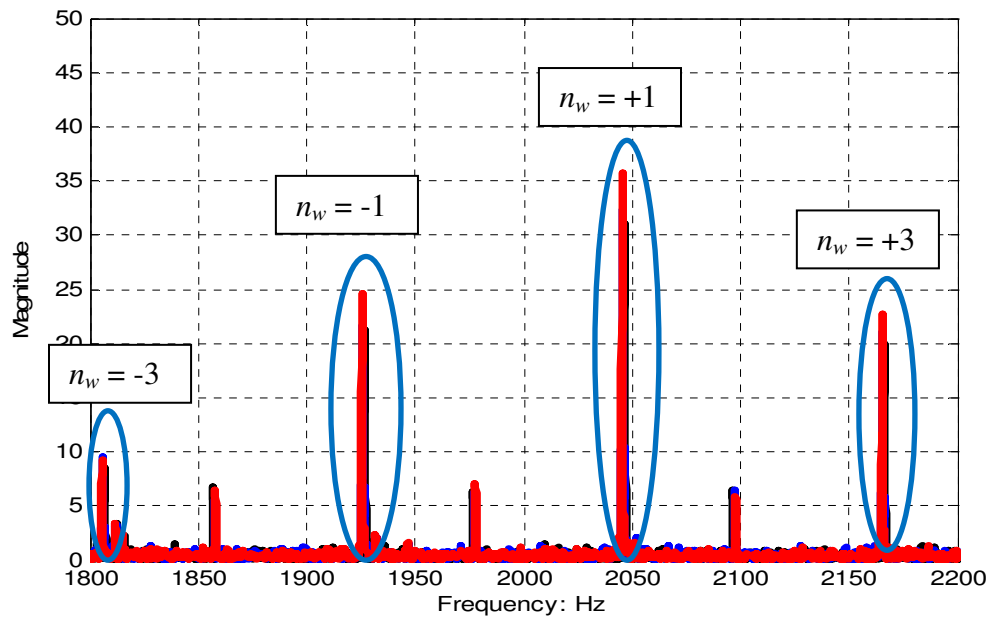
Figure 3-3: Current Spectrum for the test motor in range from 1800 Hz to 2200Hz. The signals indicated with ovals are the four rotor-slot harmonics.

The low order rotor slot harmonics are analyzed more closely below. The harmonics are presented in amplitude order, $n_w = +1$ being the strongest and -3 the weakest. Manual speed estimates were recorded using a handheld tachometer. Each labeled plot of individual slot harmonics is prefaced by a corresponding table. Equation 3-1 is used to calculate where that particular harmonic is expected in the current spectrum. The actual slot harmonic location is also recorded for comparison. In each case, the slot harmonic estimate differs less than two tenths of a percent from the expected value.

Table 3-3: Slot harmonic Comparison for $n_w = +1$

	Speed	Expected f_{sh}	Actual f_{sh} =
Reference	3512	2050.1	2047.3
With 10g added	3511	2049.6	2046
With 13g added	3510	2049	2045.5
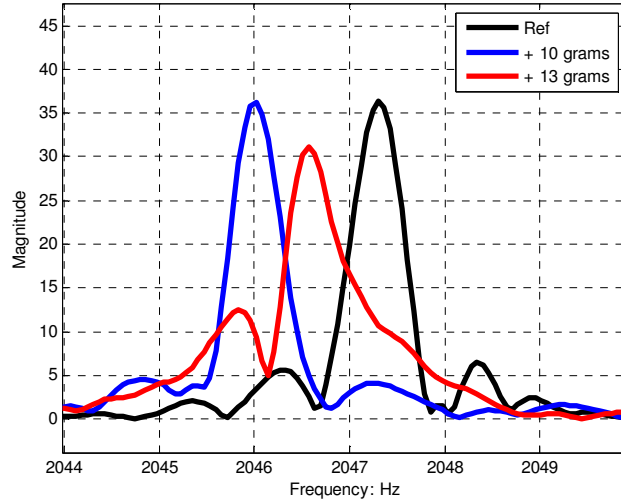
Figure 3-4: Slot Harmonic ($n_w = +1$)

Table 3-4: Slot harmonic Comparison for $n_w = -1$

	Speed	Expected f_{sh}	Actual f_{sh} =
Reference	3512	1930.1	1927.3
With 10g added	3511	1929.6	1926
With 13g added	3510	1929	1926.5
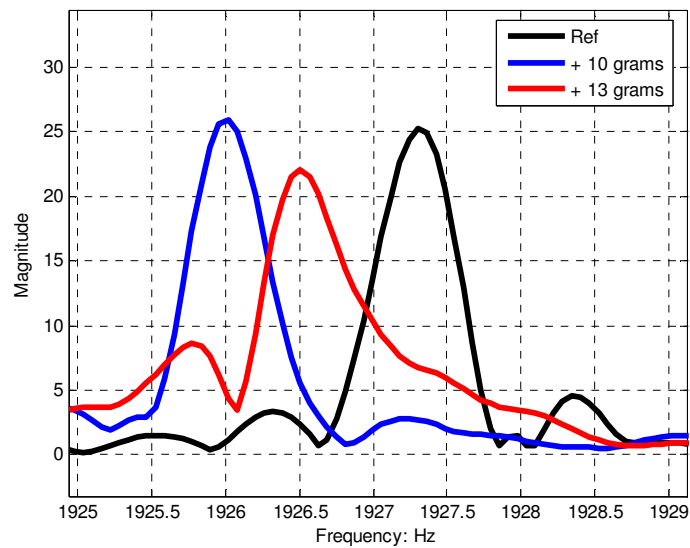
Figure 3-5: Slot Harmonic ($n_w = -1$)

46

Table 3-5: Slot harmonic Comparison for $n_w = +3$

	Speed	Expected f_{sh}	Actual f_{sh} =
Reference	3512	2170.1	2167.3
With 10g added	3511	2169.6	2166
With 13g added	3510	2169	2166.7
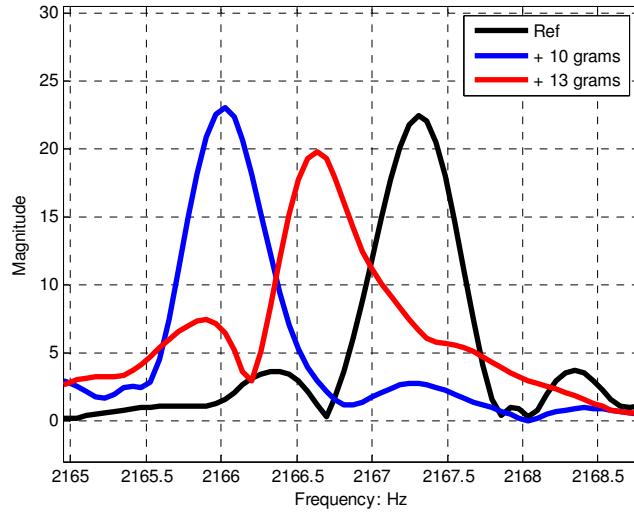
Figure 3-6: Slot Harmonic ($n_w = +3$)

Table 3-6: Slot harmonic Comparison for $n_w = -3$

	Speed	Expected f_{sh}	Actual f_{sh} =
Reference	3512	1810.1	1807.3
With 10g added	3511	1809.6	1806
With 13g added	3510	1809	1806.4
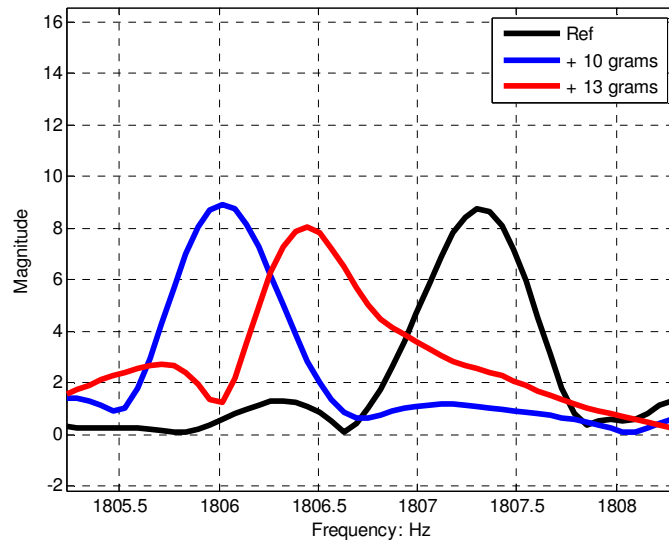
Figure 3-7: Slot Harmonic ($n_w = -3$)

There is a small but relatively consistent shift between the calculated value and actual value for each set of slot harmonics. This shift could be due to a slight variance in supply frequency (f_1) or the result of manual speed measurement. This particular test was performed at approximately 1:00pm on a week day, a time when the power grid typically experiences a heavier load. It is possible that the supply frequency may have dipped slightly during this test. For example, a frequency dip of 0.1 Hz results in a 3 Hz decrease in slot harmonic frequency in the current spectrum. In order to develop an automated speed detection algorithm it may be necessary to determine the expected supply frequency variation. This problem could be eliminated altogether by using the current spectrum to determine supply frequency instead of relying on user input. In marine applications this variation can be significant and should be taken into account.

It appears that each of the variables in Eq. 3-1 can be assumed constant given a specific situation with the exception of slip. To initially find the slot harmonics, a search window could be set to start at the point of zero slip and moved down the current spectrum. Once the spike is detected that value of slip used to position the search window would be recorded and used in near real time diagnostic calculations.

3.6   Detecting Faults using Current Spectral Quantities

3.6.1   *Mechanical Imbalance*

The first source of harmonics injected into the stator current of an induction machine originates from cyclical load torque variation or torque modulation. These position-dependent changes in torque are common in electromechanical loads. The frequencies at which these components are produced in the stator current are predicted by Eq. 3-3. In this equation, F_1 is the fundamental supply frequency, s is the slip, p is the number of poles, and m is an integer value [26].

$$F_{load} = F_1\left[1 \pm m\left(\frac{1-s}{\frac{p}{2}}\right)\right]$$

(3-3)

Observing these stator current harmonics is the first step toward confirming the NILM's ability to reliably detect more complex load and bearing problems. To verify the NILM's ability to detect cyclical load torque variation the axial fan used to produce the slot harmonics above will be used to verify two modes of imbalance and verify their presence with the vibration spectrum.

Vibration monitoring is currently the primary method used to detect the presence of fault conditions in induction machines. The mechanical vibrations are associated with variations in the physical air gap of the machine and stator currents are generated at predictable frequencies related to the electrical supply and vibration frequencies [18]. This section will confirm the value of current monitoring for induction machines by correlating the relationship between

vibration and current frequencies caused by known imposed induction machine faults (e.g. imbalance and bearing faults).

To record vibration, a medium size vibration sensor was mounted on the outside of the axial fan housing as depicted in Fig. 3-8. This orientation was selected using the standard portable vibration recorder (STS-101) operating procedure employed by the Coast Guard intermediate maintenance activity [27]. This sensor was not used to provide empirical amplitude data but simply used to establish position in the vibration spectrum and show relative amplitude changes between known conditions. This specific "geo" sensor is large enough to produce a current that can be wired directly into a NILM channel and processed in parallel with current data. Thus, both vibration data and current spectrum data will be presented in parallel and represent identical moments in time.

Figure 3-8: Vibration Sensor Mount

Equation 3-4 and 3-5 below provide a framework for implementing two different modes of imbalance, mass variation and radial location variations.

$$T_{load} = T_{initial} + T_1 sin(2\pi f_{ecc} t) \tag{3-4}$$

$$T_1 = mgr \tag{3-5}$$

It is expected that an increase in T_1 due to an increase in mass or radial distance from the axis of rotation will result in a proportional increase in T_{load}. Unbalanced loads will cause motor torque to vary as indicated where m is mass of the imbalance, g is the gravitational constant, and r is the radial distance of the mass from the axis of rotation.

This first test looks at the NILMs ability to detect cyclical load torque variations by varying mass and keeping the location of the mass or radius constant. T_1 is expected to vary proportionally with mass resulting in a proportional increase in the total torque load of the motor.

Figure 3-9 shows the methodology used to imbalance the impellor. Because the impellor is spinning at nearly 3600 RPM it was important to ensure that the mass was secure. Simply adding bolts of varying length to vacant treaded holes in the hub was the safest and most economical way to perform these tests.

Figure 3-9: Axial Fan Imbalance Method (magnitude)

Entering Eq. 3-3 with known parameters, supply frequency (f_1 = 60 Hz), harmonic number (k = 1), number of poles (p = 2) and slip (s) is calculated with Eq. 3-2 to be 0.024, resulting in a calculated f_{ecc} = 118.5 Hz. The relationship between physical vibrations and the current spectrum can be expressed by Eq. 3-6 where k is chosen to be 1.

$$f_{ecc} = |f_1 \pm k * f_{vibration}|$$
(3-6)

Entering Eq. 3-6 with known values for f_{ecc}, f_1, and k, the frequency of vibration can be predicted at 118.5 – 60 or 58.5 Hz in the vibration spectrum.

Three tests were run in this set, the first was a reference (no weight added), a test with 7 grams was added 1" away from the axis of rotation, and a test with 10 grams added 1" away from the axis of rotation. Figure 3-10a and b presents the resulting vibration and current spectrums respectively. This test confirms the expected location and amplitude relationship using the vibration spectrum.
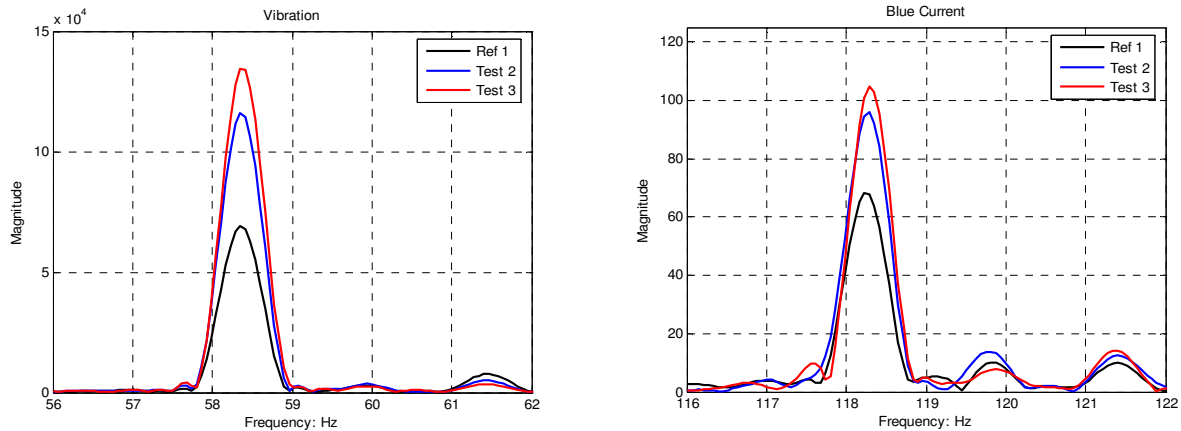
Figure 3-10a and b: Varying Mass Test Vibration and Current Eccentricity

.

The next test performed assess the NILM's ability to monitor an induction machine imbalance using a constant mass but varying the location with respect to the center of axial rotation. A 6.8 gram calibrated fan weight from a vibration analysis kit at the Coast Guard Industrial Electrical Shop was used to induce a vibration as shown in Fig. 3-11. The weights are "C" type which can be moved along the leading edge of the impellor blades. Three tests were recorded, the first test represented a reference with no weight added, the second placed the weight 3" from the center of rotation and the final test moved the same weight to a position 3.25" from the center of rotation. Figure 3-11 on the following page presents a weighted run with the weight 3" from the axis of rotation. This test is significant because this showed how the NILM could be potentially used to detect misalignments and changes in alignment.
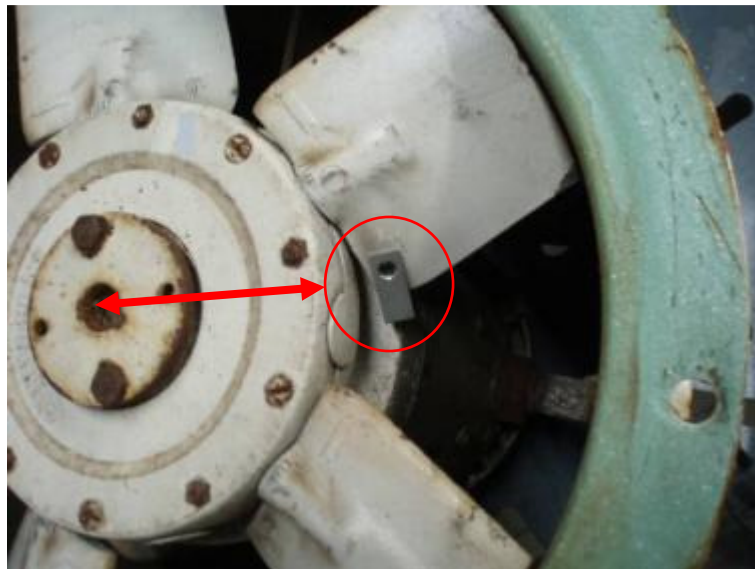
Figure 3-11: Fan with 6.8 gram weight 3 inches from center

Figure 3-12: Axial fan test

A laser tachometer was used to monitor the speed of the fan for each run. The speed of the fan remained relatively constant (3507 RPM) over each test. Using Eq. 3-3, the eccentricity frequency (f_{ecc}) for the fan was calculated to be 118.45 Hz. According to Eq. 3-2 and 3-3, a linear relationship should exist between the eccentricity component amplitude and imbalance weight distance from axis of rotation or radius r.
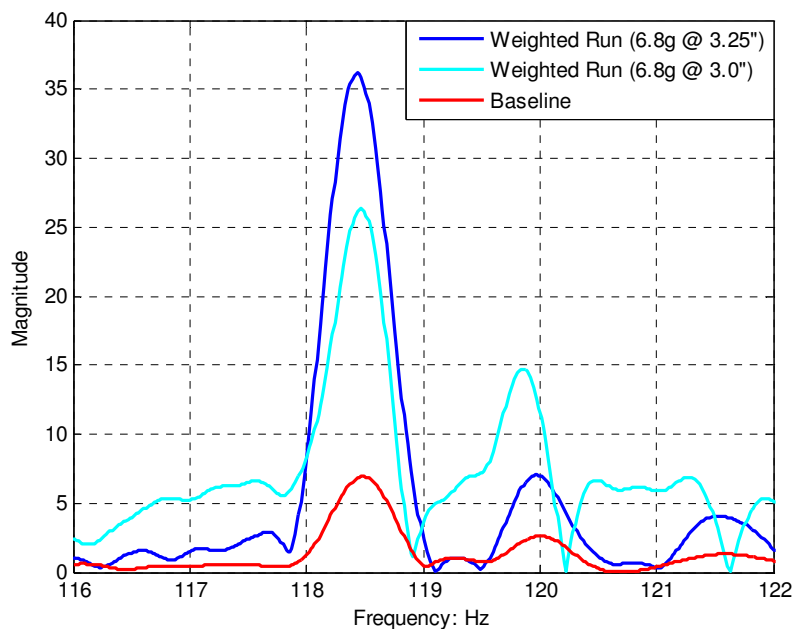
Figure 3-13: Eccentricity comparison based on radial location

Figure 3-13 presents the results of the three tests. If these measured eccentricities are assumed to be linear then the total system response can be considered a sum of simple linear

52

responses. This test confirms the NILM's ability to detect radial changes in weight imbalance and it reflects the proportionality of Eq. 3-4 and 3-5 within reason.

3.6.2 *Motor Bearing Damage Detection*

Numerous studies have shown that bearing problems account for over 40% of all machine failures in large machinery applications [16], [25].   There is strong evidence that stator current monitoring can provide bearing health indications similar to typical vibration analysis without having to access the motor. A significant amount of work has been done demonstrating the feasibility of detecting specific bearing faults by correlating characteristic bearing frequencies to the spectral components of the stator current [18],[28]. Monitoring of roller bearings is very important in applications where failure would result in loss of human life or replacement would require long production downtimes.

This series of tests seeks to confirm that it is possible to use characteristic bearing frequencies in the current spectrum to find bearing degradation. This is possible because defective bearings generate mechanical vibrations at the rotational speeds of each component in the bearing. These characteristic frequencies, which are related to the inner or outer raceways and / or balls or roller geometry, can be calculated. Still today mechanical vibration analysis techniques are used to monitor these frequencies in order to determine machine bearing health. The relationship of the bearing vibration to the stator current spectrum can be determined by recalling that any air gap eccentricity produces anomalies in the air gap flux density [29].   The test in this section attempt to confirm that the NILM can detect the initial signs of bearing damage and ultimately bearing failure.

By knowing bearing geometry and the speed of the induction machine, specific bearing problems can be predicted and located (e.g. inner / outer raceway, specific bearings, etc.).   The same vent fan used in the last test was monitored for bearing wear testing.

3.6.2.1 *Inducing Realistic Bearing Faults*

There are a myriad of conditions that cause bearing faults in industry. Some of the most common faults are flaked running surfaces due to material fatigue, excessive clearance due to extensive wear, excessive preload conditions, and poor lubrication. Bearing material fatigue usually results in a crack created in rings and rolling elements and originates from a pre-damaged spot on the raceway / bearing or because of an inhomogeneous cast during manufacture. Damage starts below the surface and propagates to the surface of the rolling element where it causes material to break loose forming pitting in the contact areas as shown in Fig. 3-14 [29].
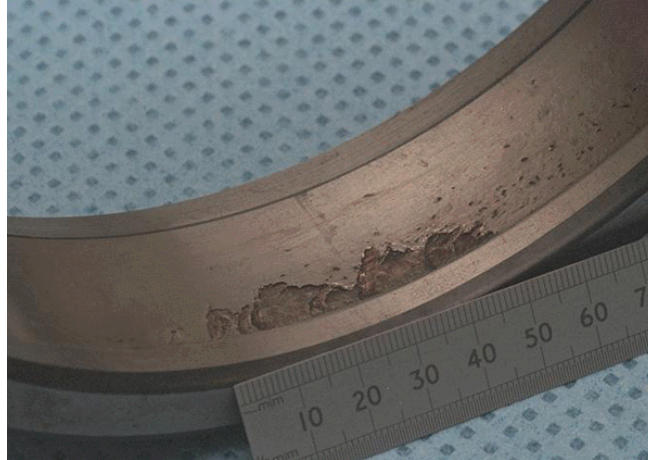
3-14: Example of Outer Race Spalling in a Deep Groove Ball Bearing

3.6.2.2   *Realistically Damaging the Inner and Outer Bearing Race*

Most small to medium bearing assemblies are machine assembled and sealed to preserve the manufacturer's lubricant and prevent foreign object intrusion. This makes it a challenge to damage a specific location in a bearing race without affecting other bearing elements. A custom clamp, vice and Dremel with a diamond tip bit was used to damage the inner and outer race in two separate 6203 bearings in a manner very similar to that seen in Fig. 3-14. Figure 3-15a, b, and c are photos of the damaging process.

Figure 3-15a,b,c: Bearing Damaging Process

The bearings were held in place using a hand vice and stationary vice while a small diamond tip bit was negotiated around the raised race edges and bearing cage. The bit was held in place long enough to remove the hardened surface of the race to a depth of between 1 and 2 millimeters. After damaging the inner and outer races the bearing need to be operated to allow time for fault development. Each of the damaged bearings was initially new with tight bearing cages and race fits. In order to wear two sets of damaged bearings simultaneously, the damaged

54

inner race bearing was installed in the non-load end and the damaged outer race bearing was installed in the shaft end of the axial fan motor. The fan was energized for approximately 10 days. Next, the motor was disassembled and the damaged bearings installed on the non-load end (bearings with inner race damage) were replaced with a new set and the motor reassembled.

Figure 3-16: Axial Motor Test Stand

The NILM was configured to monitor six channels, two recording vibration data like that used in section 3.2.2 as well as voltage and current data for two motors.

3.6.2.3 *Monitoring Bearing Race Damage*

A derivation for the bearing vibration equations can be found in [29]. The solution to the inner and outer race bearing frequency components can be found in the vibration spectrum where *n* is the number of balls in the bearing, *PD* is the bearing pitch diameter, *BD* is the ball diameter, β is the contact angle of the balls on the races and f_{rm} is the mechanical rotor speed in Hertz. Pitch diameter, ball diameter, contact angle and the number of bearings can be attained by the manufacturer. Once determined, this value must be entered into Eq. 3-9 to determine current spectrum location.

$$f_i = \frac{n}{2} f_{rm} \left[1 + \frac{BD}{PD} \cos \beta \right] \tag{3-7}$$

$$f_o = \frac{n}{2} f_{rm} \left[1 - \frac{BD}{PD} \cos \beta \right] \tag{3-8}$$

The manufacturer specifics for the 6302 bearing assembly installed are listed below:

- PD = 28.5 mm
- BD = 7.5 mm
- n = 8
- $\beta = 0$ degrees*

* After inducing damage, bearings become looser. Given the direction of force due to axial fan, it appears likely that β is between 10 and 15 degrees in these bearings.

The fan speed varied from 3510 - 3520 RPM with the damaged inner and outer race bearing test. It is important to note that the fans were oriented horizontally for the following outer and inner bearing race damage test. Given machine speed, the frequency of bearing vibration was calculated at 173Hz and the corresponding current spectrum harmonics for outer race faults was calculated at 113 Hz and 233 Hz for $k = -1$ and $k = +1$ respectively using Eq. 3-9.

$$f_{brg} = |f_1 \pm k * f_v|$$ **(3-9)**
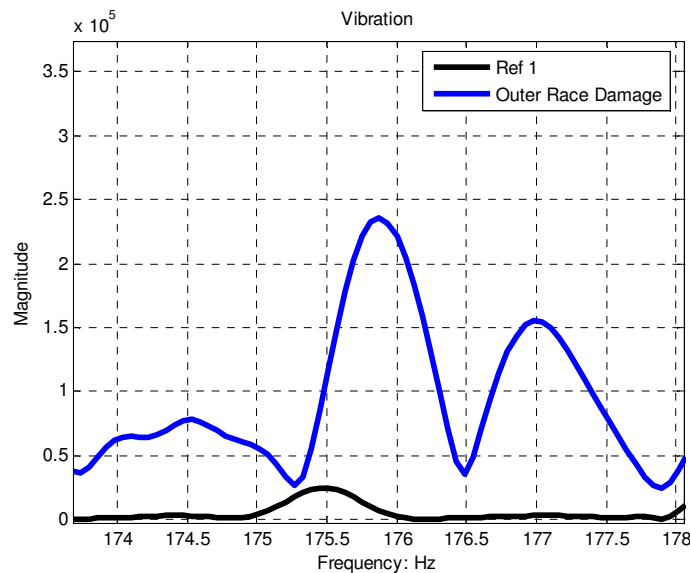
Figure 3-17: Outer Race Frequency Vibration Spectrum

The Figure 3-17 shows the vibration spectrum in the vicinity of the calculated outer race frequency. Figure 3-18, shows the current spectrum in the vicinity of the sum and difference of 60 Hz and f_v. It is difficult to determine if a corresponding signature could be identified in the current spectrum in either plot.
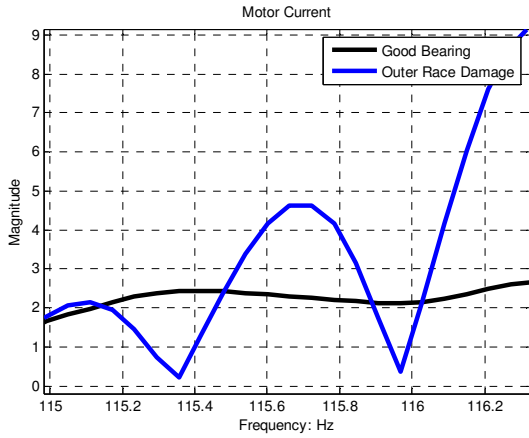
Figure 3-18: Current Spectrum (k=-1)
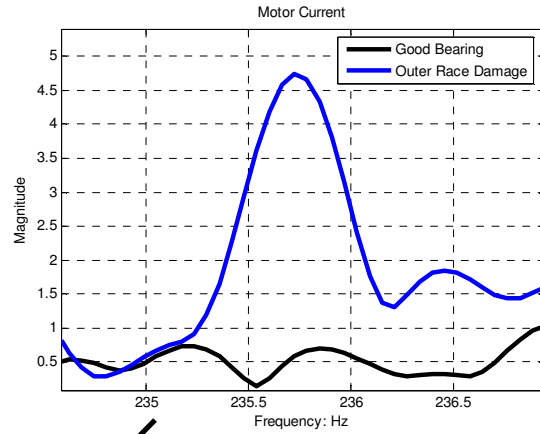
Current spectrum (k=+1)
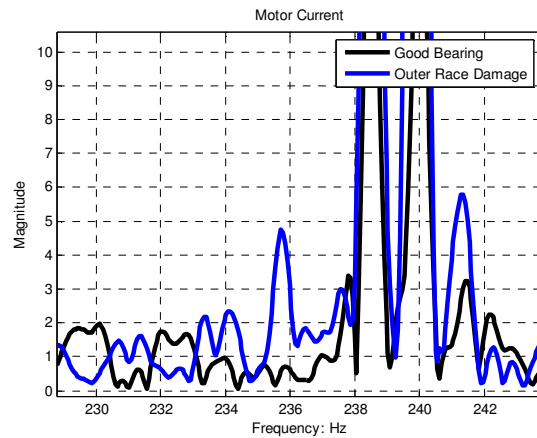
Figure 3-19: Current Spectrum (230 - 242Hz)

Unfortunately, the characteristic outer race resides very close to the second harmonic of the eccentricity frequency used earlier in this chapter to detect machine imbalance. This is a problem that could be remedied if considered in the system design phase.

The same process was used to present the damaged inner race data. Figure 3-20 and 21 on the following page presents a comparison of a good bearing and a bearing with a damaged inner ring located on the load end of the induction machine. Referring back to Eq. 3-7, the inner race characteristic frequencies are calculated to be 235 Hz and 355 Hz for $k = -1$ and $k = +1$ respectively. The inner race damage showed up much better than the outer race data and is in an optimal location in the current spectrum.
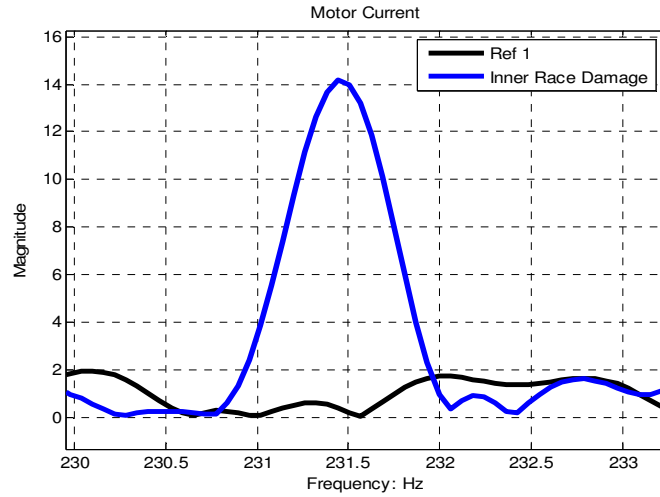
Figure 3-20: Inner Bearing Race Spectral Component (k = -1)
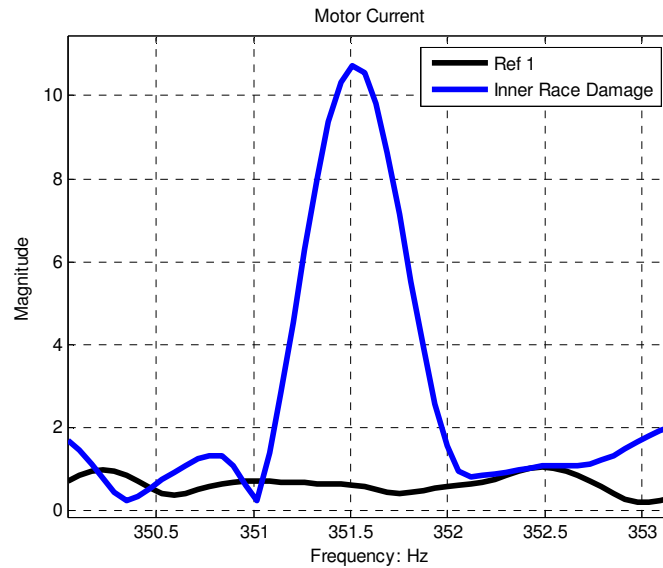
Figure 3-21: Inner Bearing Race Spectral Component (k = +1)

It is very difficult to damaging bearings in a precise manner. The difference between the amplitudes of the inner and outer race spectral components may be attributed to a number of factors such as system or equipment resonances. Regardless, the inner ring data appears strong compared to spectral comonents in the vicinity of each inner ring bearing frequency. In each presented case, the damaged bearing was installed on the shaft end of the rotor.

3.7   Impediments to Detecting Faults

3.7.1 *Pressure*

A considerable number of lessons were learned while performing the test in this chapter. The first involved test in section 3.6.1, mechanical imbalance. Originally the goal was to load the motors by restricting the airflow into the motor under test. Results were found to be inconclusive because this restriction caused such a significant change in pressure across the fan (difference between pressure at the inlet and atmospheric pressure in this case) that the eccentricities were severely damped. In comparing Fig. 3-22 on the following page and Fig. 3-10b, amplitude and separation is significantly affected by amount of pressure across an axial fan.
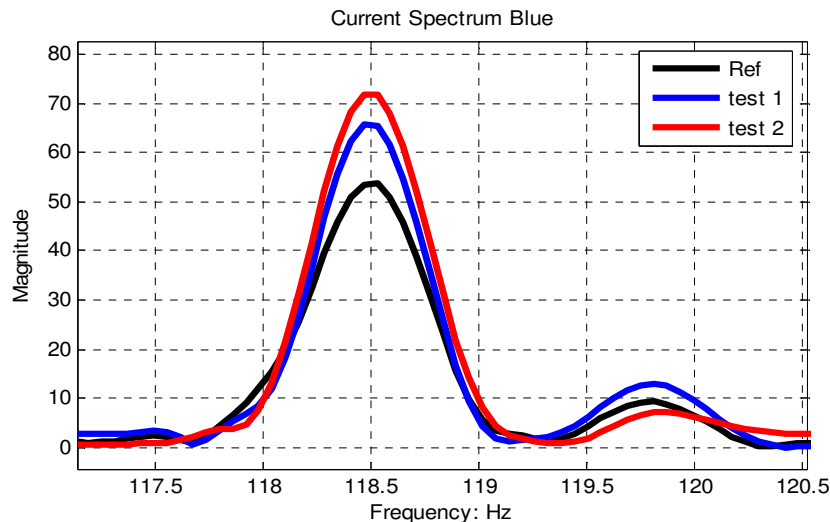
Figure 3-22:   Pressure Damped Eccentricity

3.7.2 *Orientation*

Gravity plays a significant role in detecting spectral quantities that are a function of torque variation as well as eccentricity.   This is evident considering Eq. 3-5, but the not intuitive as to how dramatic the effect might be. Initially, the bearing damage tests were conducted with the fans oriented vertically. Each test was repeated several times and a week of operation added to the bearing sets to develop the damage. Time and deepening of the race damage did little to affect the results. Figure 3-23 on the following page shows very different results while using the same bearings installed for the Fig 3-20 and 3-21 tests. The characteristic bearing frequencies at 231.5 Hz and 351.5 are hardly detectible.   In this test the bearings were installed in the shaft end of the rotor and the rotor positioned on top.
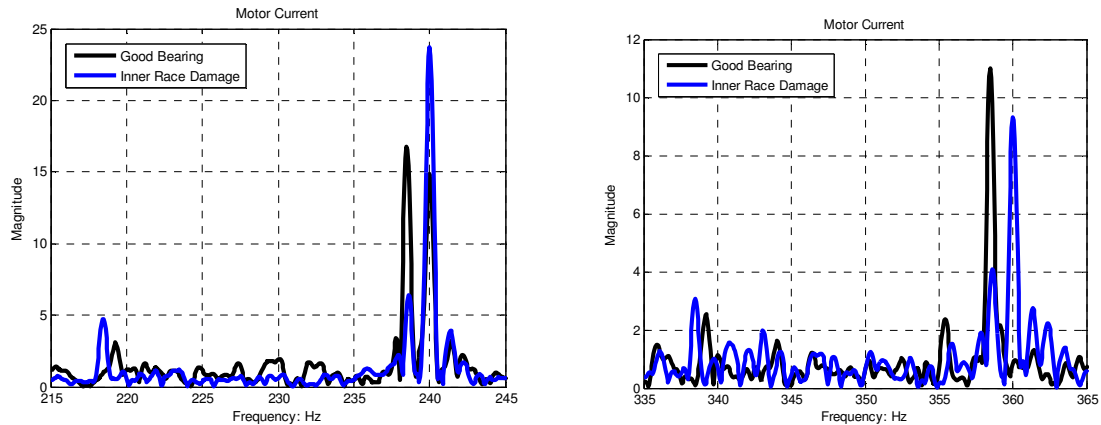
Figure 3-23: Damaged Inner Race Bearing Test with Motor Vertically Oriented

3.8   Conclusion

Multiple modes of motor damage can be detected using non-intrusive techniques. There are a significant number of factors that will contribute to the successful implementation of non-intrusive monitoring techniques. If current spectral quantities are to be used for diagnostics, effort must be made to manage the relationship between physical design characteristics and harmonics of 60Hz.   Using the example of the axial fan above, the inner bearing race characteristic frequency (235Hz) was very close to the fourth harmonic of power (240Hz). This would make automating the process depicted above more difficult. Every effort should be made to take these types of design decisions into account.

Machine loading significantly affects the signature produced by eccentric spectral quantities in the current spectrum. Again, automating a process to monitor and trend these quantities becomes much more difficult if the amplitude of these quantities varies significantly.

Induction machines are just one example of a system that current spectral quantities could be used to develop machine health diagnostics. Monitoring techniques are continually being improved. It is for this reason that current monitoring should remain a source of diagnostic information.

4 Multiple load monitoring

4.1 Laboratory Testing

The initial goal in developing the process of using a single aggregate sensor to monitor multiple loads was to start simple. Two axial fans like those used in chapter 3 with the same make and model were arranged as shown in Fig. 4-1. The test stand was built with using standard industrial shelving, additional ¾ inch plywood for additional support, and HVAC foam board to enclose part of the structure. A local MIT HVAC post doctoral researcher, Peter Armstrong, was consulted regarding ventilation intake and exhaust motor configuration and loading.
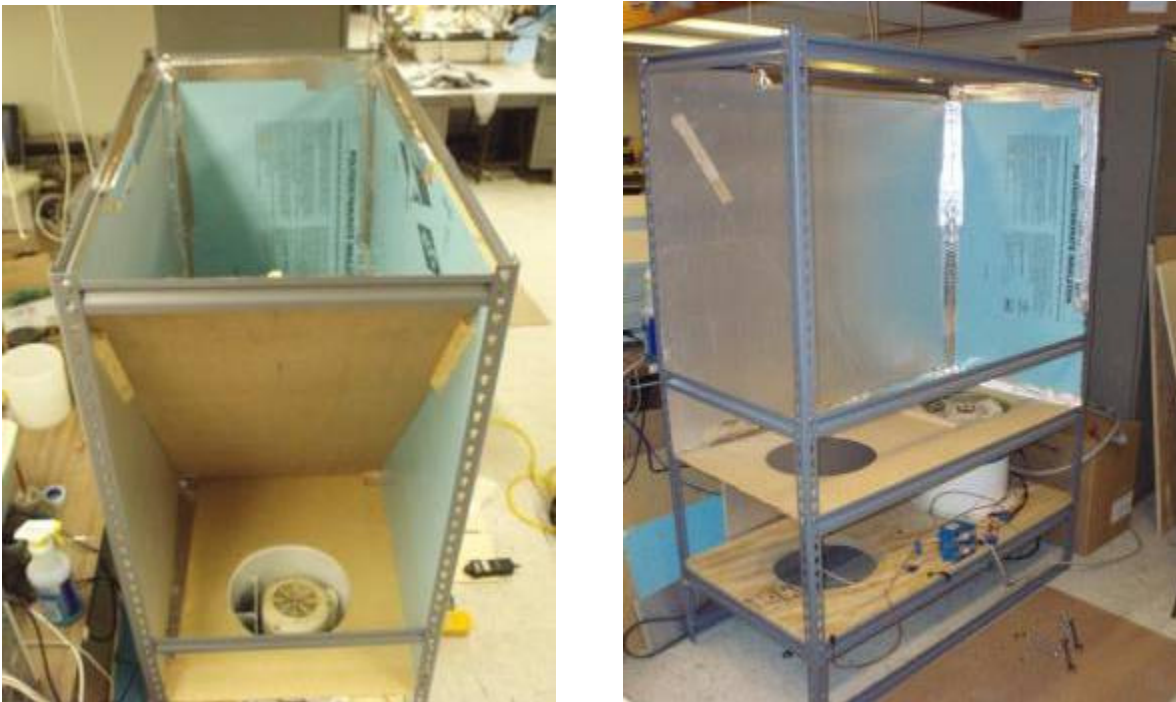
Figure 4-1: Multi-motor Test Stand

United States Coast Guard Technical Publication 2830B (WMEC 905 Class Ventilation Systems Manual) was then referenced to apply a main engine room intake and exhaust relationship to a small scale lab test. In most cases the main space intake and exhaust fans were located in the space they serviced. Therefore, the intake fan experienced the drag of ducting on the intake side of the individual motor. Conversely, the exhaust fans typically experienced slightly less drag on the discharge side of the exhaust fan. This is significant because the difference in loading provides an opportunity in an industrial setting. Many times it is cheapest to use the same motor for both intake and exhaust in industrial or marine applications because of maintenance and supply chain concerns. In this case, two identical motors loaded differently will result in each motor having a characteristic slip that can be used to identify each from a single aggregate source.

It was determined that the intake fan should be configured to experience a flow resistance similar to that resulting from a half blocked motor inlet. The exhaust fan should experience the flow resistance resulting from a quarter blocked discharge to simulate the relationship described above. Figure 4-2 is a simple diagram of the resulting setup. The material located above the vent fans was installed to prevent flow oscillations.
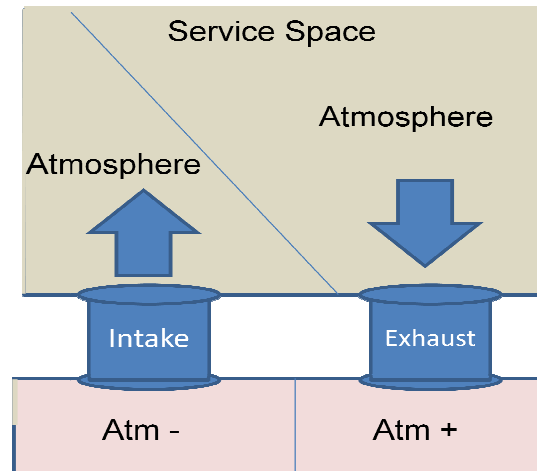
Figure 4-2: Initial Multi-motor test-stand

4.1.1 *NILM Setup*

The NILM setup in Fig. 4-3 was configured to record six channels of data. The first two channels were used to record vibrations of the exhaust motor for the reasons expressed in chapter 2. Channels 3 and 4 were used to record aggregate voltage and current respectively and channels 5 and 6 recorded only the blue motor. A block diagram of this test setup is shown in Fig. 4-4.

Figure 4-3: NILM Setup for Aggregate Sensor Testing
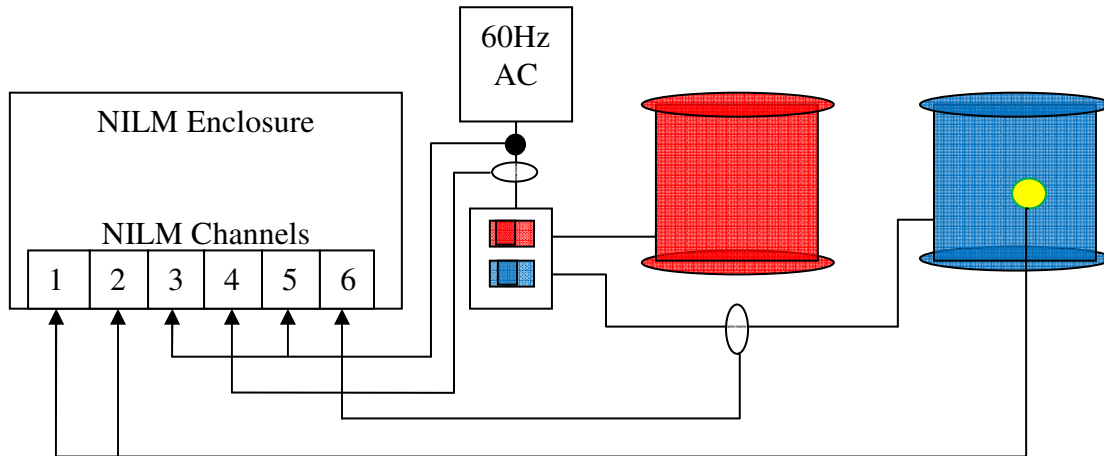
Figure 4-4: Block Diagram for Multi-motor NILM Test

The black node represents a voltage connection, an unfilled circle represents a current transducer and the highlighted circle on the blue motor represents the vibration sensor. It was necessary to use channels 3 and 5 for voltage in order to prevent a significant time lag between either aggregate or blue motor voltage current pairs. This is important for preprocessing data in the future.

4.1.2 *Modifying the Single Motor Process*

The primary difference between the single load block diagram in Fig. 3-1 and Fig. 4-5 is that key data pertaining to each individual load (e.g. number of rotor slots, number of pole pairs, etc.) is organized by load into arrays. These parameters are used to identify slot harmonics associated with a specific machine, calculate slip for that machine and pass that information with all other information known about that particular machine to the diagnostics section. Recall in the previous example, the GUI would have a data entry function where the key motor parameters for each machine under test. This parametric data is fed into the Information and Computation function and organized according to the specific induction machines feed by the load center being monitored. This function stores the key parameters and uses the slot harmonic calculation to determine slip for each induction machine. It then packages this information in vectors and passes it to the diagnostic subroutines according to preferences entered into the GUI.   This process is repeated until each of the entered loads is initially established and passes through the specified diagnostics. Figure 4-5 on the following page presents the multi-motor approach using a general block diagram. There are a number of advantages to using such a process. First, the graphical user interface (GUI) could be used to enter the number of loads, type of loads and key attributes of those loads into a computational module. Additionally, the GUI could also be used to establish or eliminate diagnostic test to performed on a specific machine or load.

63
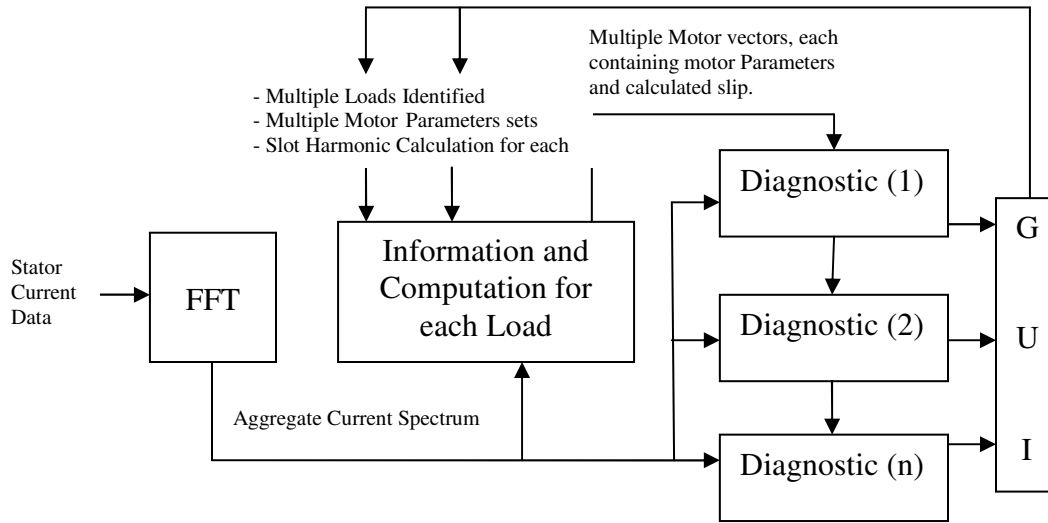
Figure 4-5: General Multi-motor Diagnostic Process Block Diagram

4.1.3 *How test were performed*

The PCI 1710 was set to sample at a rate of 48.456 kHz or 8.076 kHz per channel for 90 seconds. Once the PCI 1710 card was configured and destination directory set, both motors were energized and data recording started. After 45 seconds the red motor was secured leaving only the blue motor running. At each of the two steps, current, real power, reactive power, power factor, axial vibration and each fan's RPM were recorded. This manual data was recorded and used to confirm NILM operation.

4.2 Determining Speed of Multiple Machines using Aggregate Sensor data

Ninety seconds of raw current data was data was recorded and stored for each test conducted. To determine the feasibility of monitoring these two induction motors from an aggregate point, the eccentricity test procedure from Chapter 3 are used. Figure 4-7 shows the recorded current in the time domain. The window in the figure highlights the section of data
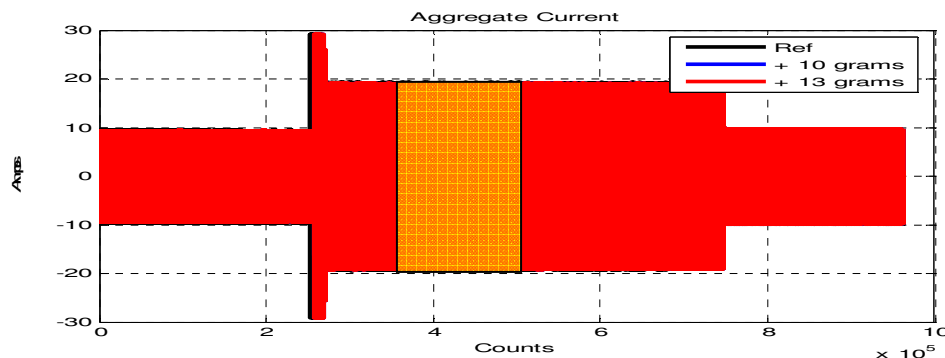
Figure 4-6: Multi-Motor Time Domain Current

64

selected to create the frequency domain plots or spectral current. There are three tests represented, a reference case with no imbalance, a case with 10 grams of weight added one inch from the axis, and a run with 13 grams added one inch from the axis. The time domain plot appears all red because the larger imbalance draws the most current. Each motor is virtually identical with the exception of slip, which should result in two definitive sets of slot harmonics near the predicted values. Each set will be used to predict the speed of each machine.

The same methodology discussed in Chapter 3 is employed. Recall Eq 3-1 shown below, the slot harmonic equation With values for f_1, R, and p known, a k value of 1 was assumed as well as static eccentricity ($n_d=0$). The same initial values in Table 3-2 were used.

$$f_{sh} = f_1 \left[(kR \pm n_d) \left(\frac{1 - s}{p} \right) \pm n_w \right]$$

<div align="center">

Table 4-1: Slot Harmonic Variables

$F_1 = 60$ Hz	$k = 1$
$R = 34$	$n_d = 0$
$p = 2$	$n_w = \pm 1, \pm 3$

</div>

At this point each of the four slot harmonics will be compared. Tables 4-2 thru 4-5 list the expected location and actual location for n_w = +1, -1, +3, and -3, respectively. Both motors corresponding slot harmonics can be seen at predicted locations in the current spectrum.
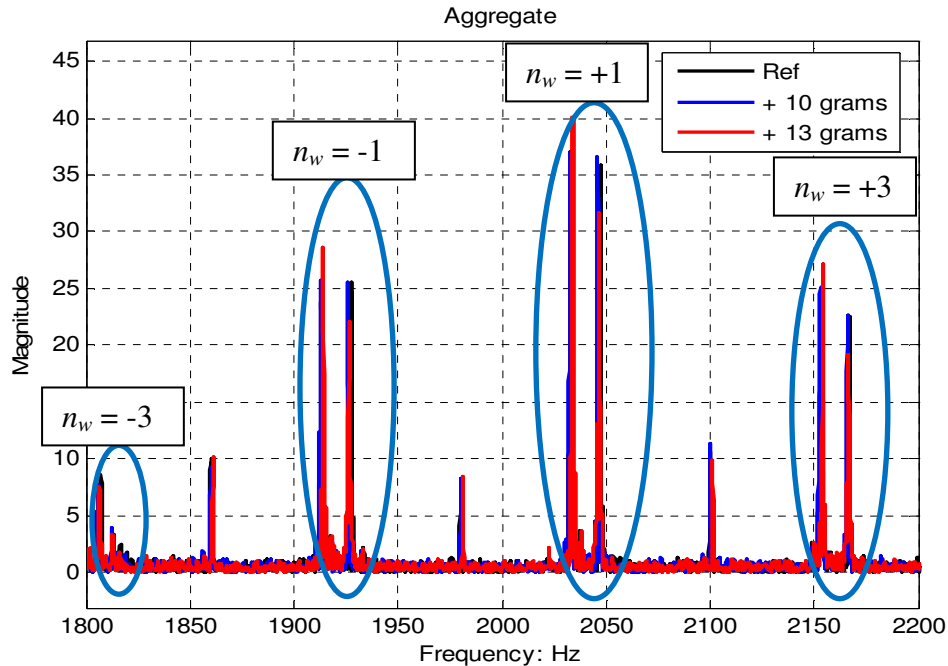
Figure 4-7: Aggregate Current Spectrum (1800 - 2200Hz)

4.2.1 *Multi-load Slot Harmonic Analysis*

The tests procedure used in Chapter 3 was performed and the aggregate current transducer data was used to create the figures below. In the n_w case, the current transducer isolating the blue motor was used to confirm similar amplitude scheme as well as location in the current spectrum. They do in fact agree as do the remaining three harmonics.

Table 4-2: Slot harmonic Comparison for n_w = +1

	Speed (Red)	Speed (Blue)	Expected f_{sh} (Red)	Actual f_{sh} = (Red)	Expected f_{sh} (Blue)	Actual f_{sh} = (Red)
Reference	3482	3508	2033	2032.5	2047	2047.4
With 10g added	3480	3503	2032	2032.6	2045	2046
With 13g added	3485	3505	2035	2034	2046	2046.8
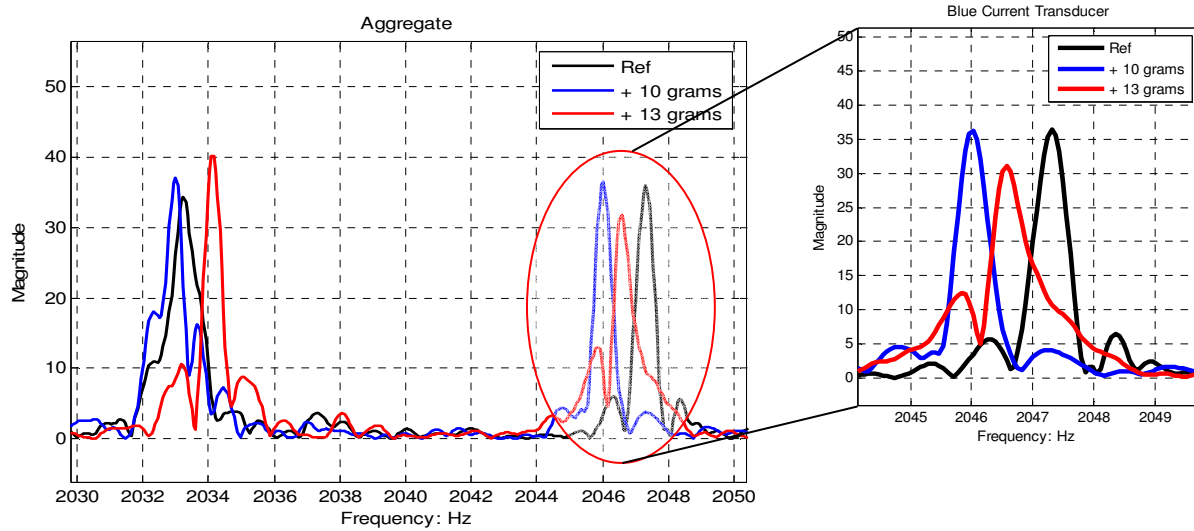
Figure 4-8: Slot Harmonic (n_w = +1)

Table 4-3: Slot harmonic Comparison for n_w = -1

	Speed (Red)	Speed (Blue)	Expected f_{sh} (Red)	Expected f_{sh} (Blue)	Actual f_{sh} = (Red)	Actual f_{sh} = (Blue)
Reference	3482	3508	1913	1928	1913	1927.3
With 10g added	3480	3503	1912	1925	1913	1926
With 13g added	3485	3505	1915	1926	1914	1927
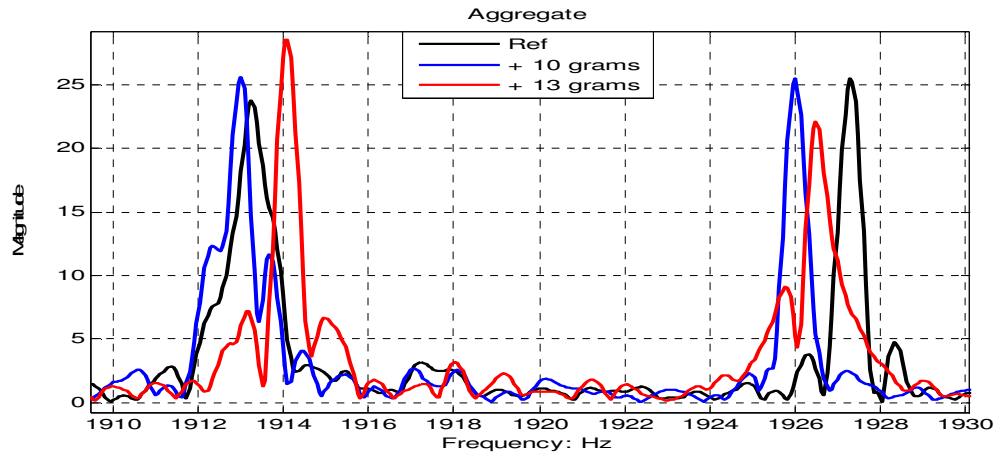
Figure 4-9: Slot Harmonic (n_w = -1)

Table 4-4: Slot harmonic Comparison for n_w = +3

	Speed (Red)	Speed (Blue)	Expected f_{sh} (Red)	Expected f_{sh} (Blue)	Actual f_{sh} = (Red)	Actual f_{sh} = (Red)
Reference	3482	3508	2153	2168	2153.2	2167.3
With 10g added	3480	3503	2152	2165	2153	2166
With 13g added	3485	3505	2155	2166	2154.2	2166.8
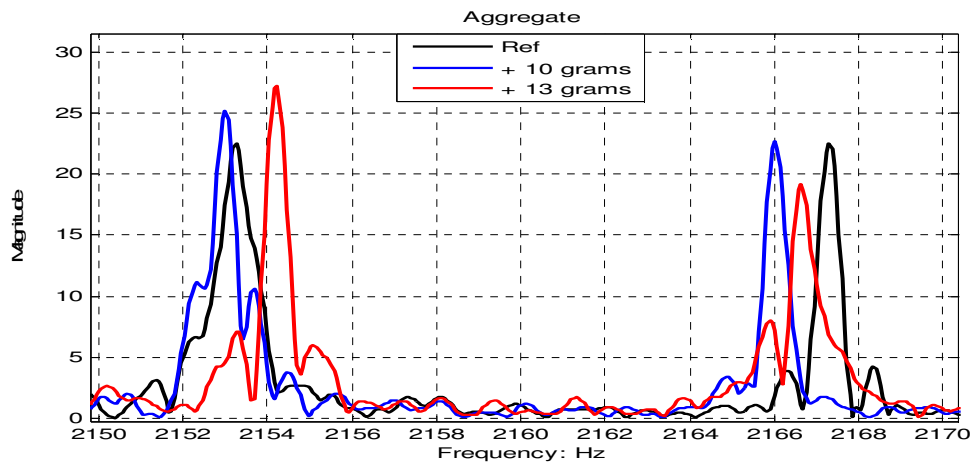
Figure 4-10: Slot Harmonic (n_w = +3)

67

Table 4-5: Slot harmonic Comparison for $n_w = -3$

	Speed (Red)	Speed (Blue)	Expected f_{sh} (Red)	Expected f_{sh} (Blue)	Actual f_{sh} = (Red)	Actual f_{sh} = (Blue)
Reference	3482	3508	1793	1808	1793.2	1807.2
With 10g added	3480	3503	1792	1805	1793	1806
With 13g added	3485	3505	1795	1806	1794	1806.5
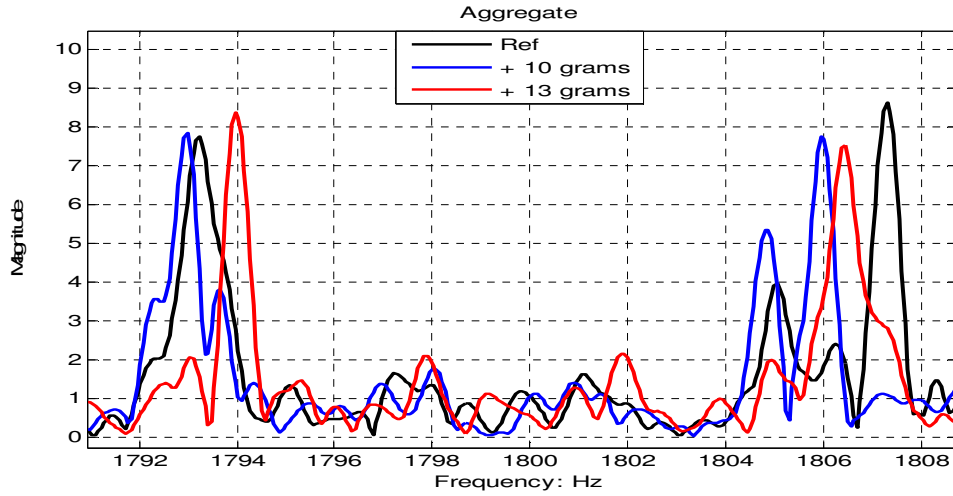
Figure 4-11: Slot Harmonic ($n_w = -3$)

The slot harmonics for these four cases show up relatively consistently within a Hertz of the expected value. Tachometer readings of both motors varied by $\pm$ 1 RPM. Therefore, an average value was used. The most significant error was less than $1/10^{th}$ of a percent, which is extremely accurate by most standards. The amplitude does not seem to provide any definitive information for this particular set of test. Additionally, there does not appear to be a relationship between imbalance and slip.

There are limitations to this particular monitoring scheme. It is proposed in this chapter that slot harmonics be used to determine speeds of multiple motors to populate a slip array (s_1, s_2,..., s_n) where n = number of motors supplied by the load center.   In this scenario, two near identical motors are operating at close to the same speed. Consider the case above with a 13 gram imbalance; the red motor is defined as motor 1 and blue motor defined as motor 2.   Using the slot harmonic determined slip value for each would result in $s_1 = 0.9675$ and $s_2 = 0.9739$. Inserting those values into the cyclical load torque equation (Eq. 3-3) used earlier and represented below, result in $F_{load\_1} = 118.05$ and $f_{load\_2} = 118.4$.

$$F_{load} = F_1 \left[1 \pm m \left(\frac{1-s}{\frac{p}{2}} \right) \right]$$

The separation between these two spectral components is less than one half of a Hertz and would be nearly impossible to reliably differentiate with diagnostic software. Figure 4-13 presents the actual plot of the aggregate cyclical load component scenario described above.
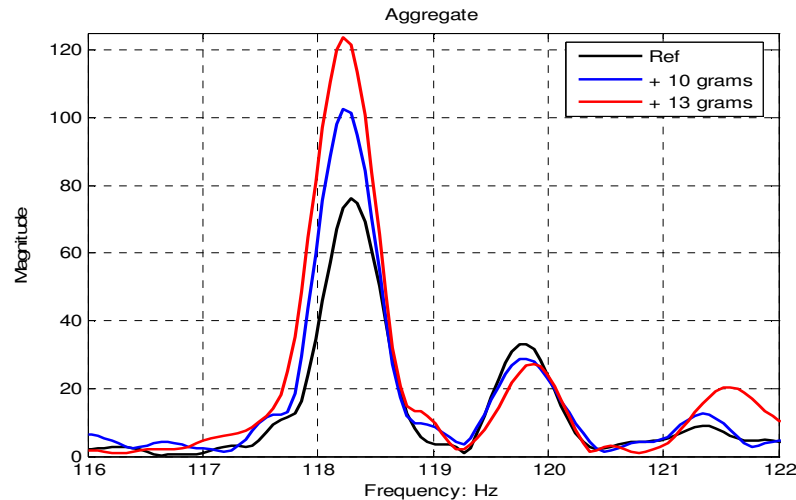
Figure 4-12: Scenario Aggregate Current Spectrum plot of Cyclical Load Component

In order to monitor two identical motors from the same source, it will be necessary to incorporate a subsequent test procedure to identify which of the two identical loads was experiencing irregularities. The NILM could still alert an operator and / or technician of irregularities but in this case would need to take additional actions to pinpoint the irregularity. The same can be shown for the bearing scenario as well.

4.2.2   *Design Options*

This test using two near identical induction machines represents a very difficult scenario. However, with the knowledge of how the current spectrum and slot harmonics can be used to identify motors, a designer could choose a design that took NILM capabilities into account. Some shipboard HVAC systems are already moving toward more NILM friendly architectures. Because the intake and exhaust vent fans are typically loaded differently, some naval architects are using that fact to choose optimal sizes for these vent fans. The majority of these cases results in larger intake and smaller exhaust vent fans, which potentially presents a better opportunity to differentiate the machines using the current spectrum.

Many new ships are automating main engineering space HVAC systems altogether. For example, the 87 ft Marine Protector Class pictured in Fig. 4-14, employs a 24 inch, 2 ½ HP axial fan intake to service the main engine room and a 15 inch, 1 HP axial exhaust fan, both which can be seen in figure 4-15. Each is operated by a variable speed drive which can be set manually with the panel in Fig. 4-16 or automatically based on main engine loading. In this case, it is much more likely that these fans do not have an identical number of rotor slots and pole pairs.

Figure 4-13: USCGC Flying Fish

Figure 4-14: Fan Control Interface Panel
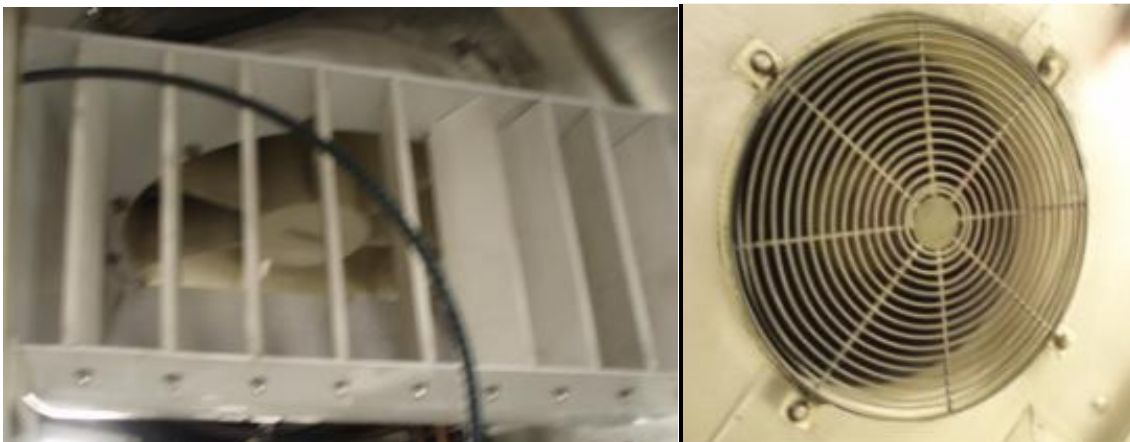
Figure 4-15: Main Engine Room Intake and Exhaust Ventilation Fans

70

4.3   Conclusions

It is possible to use spectral quantities to monitor multiple induction machine loads with one current sensor. Special techniques may be required in order to determine the specific induction machine causing elevated spectral quantities associated with system health problems. The key factors in monitoring multiple induction machines with an aggregate sensor are number of rotor slots, number of pole pairs, and load schedule or environment of each. In an ideal world, a diagnostic for monitoring multiple motors from one load center would be able to monitor a specific cyclical load torque spectral quantities for each induction machine. Depending on what the induction machine is driving, this may or may not be possible.

5 Moving to a new NILM Architecture

5.1 NILM System Architecture

This chapter will analyze the general NILM architecture prior to June 2007, when this thesis was started, and present a new architecture using tools and knowledge presented in the System Design and Management (SDM) curriculum. The original architecture will be called first generation henceforth and the emerging architecture will be referred to as second generation. The second generation architecture presented in this chapter represents the work of MIT Prof. Steve Leeb, UNC Prof. Robert Cox, Dr. Jon Rodriguez of NemoMetrics, LCDR Ethan Proper, LT Perry Branch, and the author. Refer to [19] for additional technical details relating to the first generation NILM. The resulting architecture will be presented at the same technical level as the first generation NILM is introduced.

In order to move to a new architecture, the first generation hardware will be analyzed and decomposed. The goal of the NILM system from a commercial standpoint is to be developed into a robust product that delivers value at a reasonable cost to a wide range of customers. The NILM system has the potential to deliver valuable information to customers in numerous industrial settings. Because of the variance in these settings, there will be times when the priorities must be balanced, customer needs and manufacturability for example.

5.1.1 *Modeling the First Generation Architecture*

The first step taken in analyzing the first generation architecture was to map the existing concept using a general modularized OPM or Object Process Model. The intent of this initial OPM is not to synthesize the architecture from concept but to show first and second level decomposition relationships.

The OPM in figure 5-1 was developed using details from [19] and [20]. The first generation NILM setup uses the voltage measuring board and current transducer together with a power supply and wiring terminal board inside a NEMA enclosure. Outputs from the voltage board and current transducer are connected to the wiring terminal board. The terminal board uses a Small Computer System Interface (SCSI) or "skuzzy" port to interface with the PC. This port is connected directly to the analog to digital converter in the PC. A PCI 1710 analog-to-digital data card used converts an analog signal in the range of -5 V to +5V to digital "counts" in the range of 0 to 4096 amplitude levels. The inside of a standard first generation NILM NEMA enclosure can be seen in Fig. 5-1. The PC is a standard desktop machine using a standard Pentium processor, RAM, CD ROM, LCD display and keyboard. A complete system installed aboard the *CGC Escanaba* can be seen in section 5.1.2.
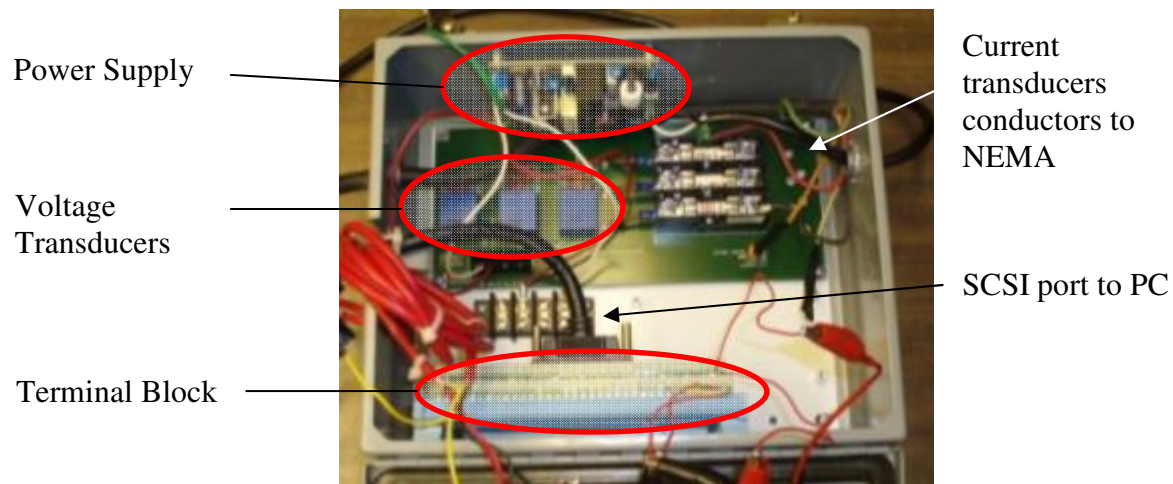
Figure 5-1: First Generation NILM NEMA Enclosure

Current transducers are located in the host or monitored load center and fed into the NEMA enclosure and ultimately to the terminal block.

Figure 5-2 represents the first order OPM that depicts these first and second level relationships.
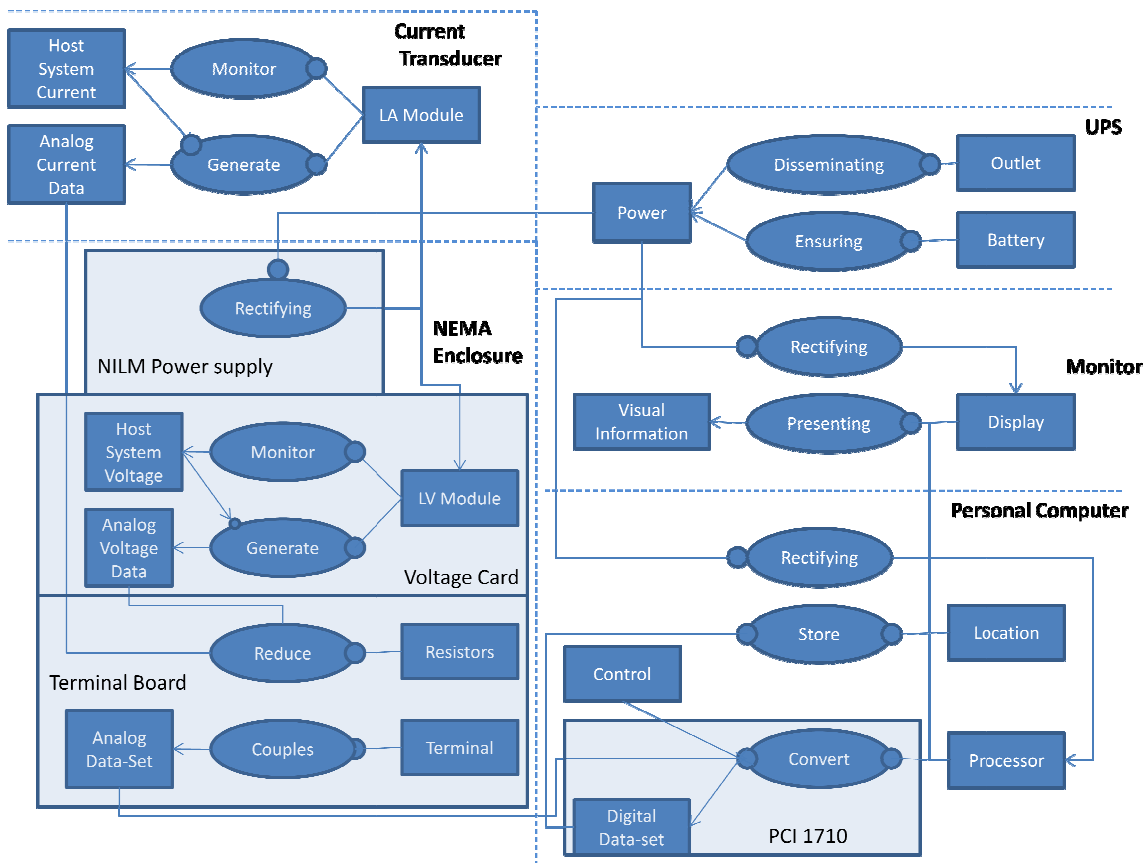
Figure 5-2: Modular Relation OPM

Stepping through the OPM development for the first generation NILM system resulted in a better understanding of sub-system boundaries. For example, it became clear that a boundary would need to be drawn between analog and digital data sets even though they could have been generally referred to as "data."

5.1.2 NILM System Decomposition

In order to enter a design tool such as a Dependency Structure Matrix a careful decomposition of the first generation system must be performed. Figure 5-3 shows a standard NILM installation. The current complete NILM system is comprised of commercially available hardware that is relatively easy to acquire, assemble, and install. Commercial or COTs hardware was initially chosen because of its wide availability and low cost. A standard first generation NILM system consists of a NEMA-type enclosure to house the voltage transducers and their associated power supply, a personal computer (PC) with keyboard and monitor, and an uninterruptible power supply. The personal computer used in NILM setups runs a Linux operating system. Linux is a very reliable system, which is especially important for system robustness. Installation of a NILM setup can be accomplished using readily available hardware and tools. For installations discussed in this thesis, the hardware was attached to panels, bulkheads, or mounting plates with nuts and bolts.
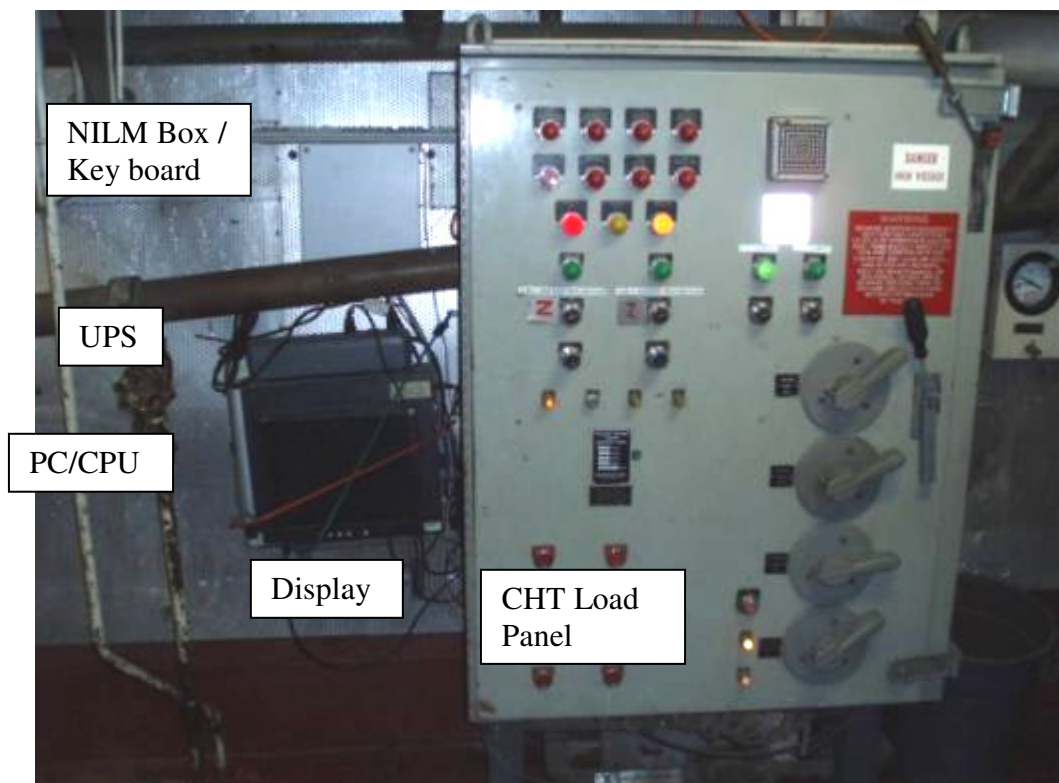
5-3: Typical NILM Equipment Installation (CGC Escanaba)

The personal computer (PC), display, uninterruptable power supply (UPS), and key board are all standard COTS hardware. The NILM box however has not had the same level of product development. Moving to a new architecture provides the team the opportunity to take a fresh look at customer needs. A block diagram of the NILM unique hardware is presented in Fig. 5-4.
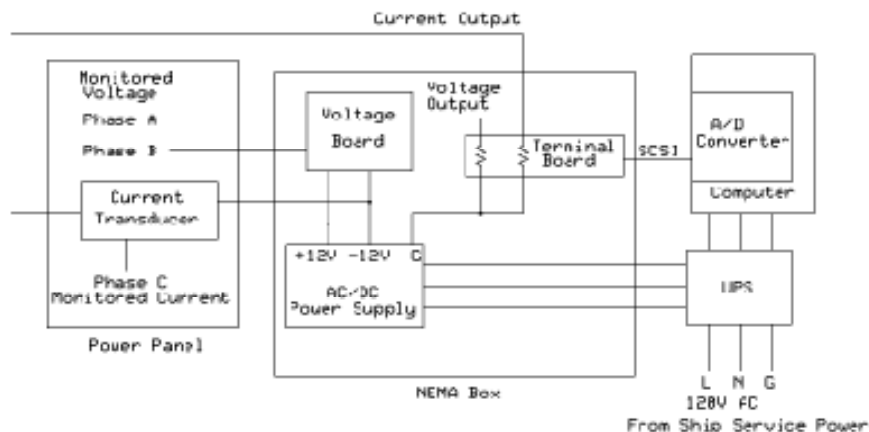
5-4: Current NILM Block Diagram

A modern Design Structure Matrix or DSM will be used to suggest a new architecture and will require a preliminary decomposition. The decomposition will need to dip down two levels prior to entering the DSM. Given that level 0 is the NILM system itself, the level 1 and 2 decomposition can be defined as depicted in Table 5-1.

Table 5-1: First Generation NILM Decomposition

First Generation NILM Level 0 Decomposition	Level 1 Decomposition	Level 2 Decomposition
System	Pentium Based PC	Power Supply (120 - 12V)
		CPU
		RAM
		CD ROM
		Hard Disk
		Video Card
		Analog - Digital Card
		Software
		Enclosure
	Display	Power Supply (120 - 12V)
		Liquid Crystal Display
		Enclosure
	UPS	Battery
		Battery Charging System
		CPU / Converter
		Enclosure
	NILM (NEMA Enclosed hardware)	Power Supply (120 - + 12 V)
		Voltage Board
		Terminal Board
		Enclosure
	Current Transducers	Current Transducers
	Standard Outlet *	Single Phase 120 V Power
	Monitored System *	Voltage Interface
		Current Interface
		Enclosure

* Only Applicable parts of these elements listed

The goal in defining specific level decomposition is to keep the parts at approximately the same level of complication. It is important to note that interconnections between the parts are not listed in the decomposition. Standard and nonstandard subsystem interfaces will be handled in the DSM instead of complicating the decomposition.

5.2 Design Structure Matrix (DSM)

5.2.1 *General DSM Mechanics*

The DSM method was chosen to synthesize the current architecture because of the existing modular design of the first generation NILM concept and element interconnections. For a quick review of how DSM works, consider a system that is composed of two elements / sub-systems (or activities/phases): element "A" and element "B". A graph may be developed to represent this system pictorially. The graph is constructed by allowing a vertex/node on the graph to represent a system element and an edge joining two nodes to represent the relationship between two system elements. The directionality of influence from one element to another is captured by an arrow instead of a simple link. The resultant graph is called a directed graph. There are three basic building blocks for describing the relationship amongst system elements: parallel (or concurrent), sequential (or dependent) and coupled (or interdependent) as shown in Fig. 5-5.

Three Configurations that Characterize a System			
Relationship	**Parallel**	**Sequential**	**Coupled**
Graph Representation			
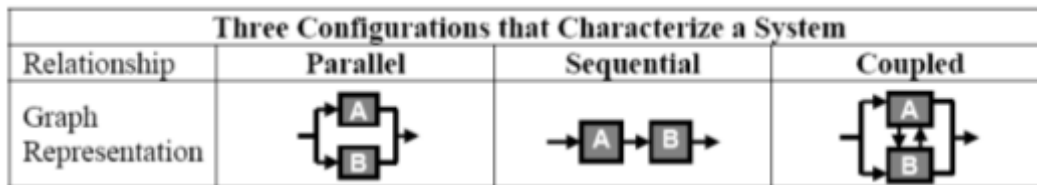
Figure 5-5: DSM relationship building blocks

The typical matrix representation of a digraph is a binary (i.e. a matrix populated with only zeros and ones) square (i.e. a matrix with equal number of rows and columns) matrix with m rows and columns, and n non-zero elements, where m is the number of nodes and n is the number of edges in the digraph. The matrix layout is as follows: the system elements names are placed down the side of the matrix as row headings and across the top as column headings in the same order. If there exists an edge from node i to node j, then the value of element ij (column i, row j) is unity (or flagged with a mark such as "X" or "●"). Otherwise, the value of the element is zero (or left empty). In the binary matrix representation of a system, the diagonal elements of the matrix do not have any interpretation in describing the system, so they are usually either left empty or blacked out as shown in Fig. 5-6 [32].

Three Configurations that Characterize a System						
Relationship	**Parallel**		**Sequential**		**Coupled**	

Figure 5-6: Binary representation

5.2.2 *DSM with expanded connections*

Working with Oliver de Weck, Professor of Aeronautics and astronautics and Engineering Systems, a DSM using an expanded connection/interface definition was applied to the first generation NILM system. This DSM was built with four sub-cells that capture the four primary types of connections / interfaces common in electromechanical systems. The connections between the elements are shown as the off-diagonal elements. Those connections include: physical connection, mass flow, energy flow (includes electrical, mechanical, or thermal flow), and information. Figure 5-7 presents a simple example of how to employ the expanded DSM.
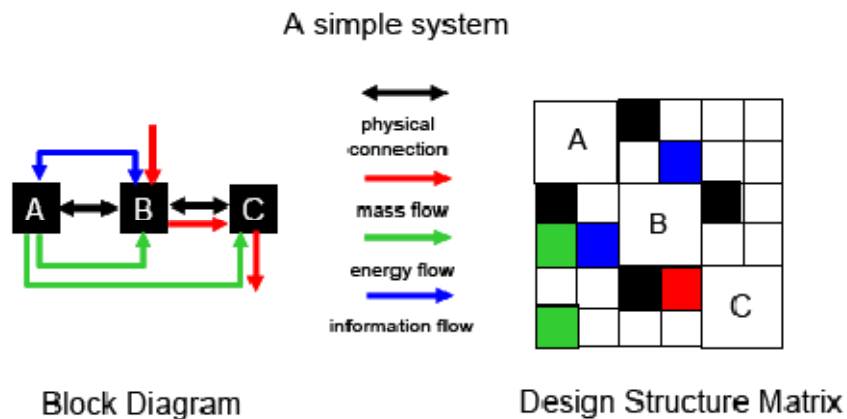
Figure 5-7: Expanded Connections DSM Example [32]

Component A physically connects to B which in turn is connected to C. A mass flow occurs from B to C, while energy is supplied from A to B and C, respectively. Additionally, A and B exchange information with each other. Such a DSM forms the basic information upon which the subsequent analysis builds.

Each of the level 2 parameters was entered into the expanded DSM according to the inter-relationships described below. The goal of this DSM will be to analyze and critique the first generation architecture and suggest an improved architecture. Table 5-2 represents an expanded DSM with first generation NILM architecture entered prior to partitioning.

Table 5-2: DSM with expanded Interconnections / Interfaces

NILM Baseline DSM Configuration

Column headers: PC Power Supply, PC CPU, PC RAM, PC Hard Disk, PC CD ROM, PC Video Card, Software, A / D Converter, PC Enclosure, LCD Power Supply, LCD Display, LCD Enclosure, UPS Battery, UPS Charging Sub-sys, UPS Enclosure, NILM Power Sup., NILM Voltage Brd, NILM Terminal Brd, NILM / NEMA Encl, Current Transducers, Data (analog), Data (digital), Single Phase Power, Target Voltage Ter., Target Current Int., Target Encl.

Row headers: PC Power Supply, PC CPU, PC RAM, PC Hard Disk, PC CD ROM, PC Video Card, Sortware, A / D Converter, PC Enclosure, LCD Power Supply, LCD Display, LCD Enclosure, UPS Battery, UPS Charging Sub-sys, UPS Enclosure, NILM Power Supply, NILM Voltage Board, NILM Terminal Board, NILM / NEMA Enclosure, Current Transducers, Data (analog), Data (digital), Single Phase Power, Target Voltage Terminal, Target Current Interface, Target System Enclosure

Groupings: Personal Computer, LCD, UPS, First Generation NILM, Monitored System

Legend:
- Physical connection (black)
- Mass flow (red)
- Energy flow (green)
- Information flow (blue)

Each position that would ordinarily represent a standard connection or interface has been sub-divided into four positions. Starting in the upper left corner and working clockwise the positions represent Physical connection, Mass flow, Information flow, and Power flow. The NILM system in its current form does not have any Mass flow connections. In order to keep the data entry and subsequent partitioning as simple as possible, some standards for data entry were observed.

They are as follows:

- If energy or information flow depended on using a standard interface both physical connection and flow connection was entered in the corresponding intersection.

- Any design dependency was considered a two way dependency. This is always the case for physical connections but is also true for some power and information sub-systems. For example, the PC power supply depends on the UPS enclosure for a connection and the size of the UPS enclosure depends on PC power requirements.

Effort was made to ensure all like subsystems are made dependent. For example, all similar power supplies are made dependent to one source. The design team also decided that the NILM system should have the ability to draw power from the target system instead of needing a separate power source. For example, most target shipboard systems use three phase 440V power. A step-down transformer of some kind could be used to deliver 110V single phase power and eliminate a requirement to have extension cords run across the engineering spaces. In order to represent this, a physical dependency was established prior to partitioning between the target system and the single phase power used to power NILM loads. With these adjustments made, the matrix was partitioned.

5.2.3 *Partitioned DSM Results*

Table 5-3: Partitioned DSM

NILM Baseline DSM Configuration	(matrix)

Legend:
- Physical connection
- Mass flow
- Energy flow
- Information flow

Consumer Off-The-Shelf (COTS) Hardware

Used to represent desire to draw power from target or host system

New Target System Definintion

New NILM box

Rows of matrix: PC Power Supply, PC CPU, PC RAM, PC Hard Disk, PC CD ROM, PC Video Card, Sortware, PC Enclosure, LCD Power Supply, LCD Display, LCD Enclosure, UPS Battery, UPS Charging Sub-sys, UPS Enclosure, Target System Enclosure, Target Voltage Terminal, Single Phase Power, Target Current Interface, Current Transducers, NILM Power Supply, NILM Voltage Board, NILM Terminal Board, NILM / NEMA Enclosure, Data (analog), A / D Converter, Data (digital)

Columns of matrix: PC Power Supply, PC CPU, PC RAM, PC Hard Disk, PC CD ROM, PC Video Card, Software, PC Enclosure, LCD Power Supply, LCD Display, LCD Enclosre, UPS Battery, UPS Charging Sub-sy, UPS Enclosure, Target Encl., Target Voltage Ter., Single Phase Power, Target Current Int., Current Transducers, NILM Power Sup., NILM Voltage Brd, NILM Terminal Brd, NILM / NEMA Encl, Data (analog), A / D Converter, Data (digital).

Table 5-3 represents the partitioned DSM. The partitioned matrix presents a reduced number of sub-systems or reduced level 1 decomposition, now there appear to be three sub-systems. The main subsystem in the upper-right has combined the PC, Display, and UPS sub-systems, followed by the target or monitored system and finally the new NEMA enclosure

5.3   Implementing Results

5.3.1   *COTS Hardware*

At this point the team began investigating how they could move forward with selecting hardware to fulfill the needs of each sub-system. COTS systems have been successfully employed to handle the processing and display functions aboard ship. The team met with the end users and engineering leadership to determine specific needs. At the same time, diagnostic software was being developed that would enable near real time monitoring of target systems. The resulting needs of the new COTS hardware component were:

- Able to run Linux and Windows environment
- Small footprint in the engineering spaces
- Out of the way
- Water resistant
- Ethernet compatibility
- Touch screen
- Easy to mount / and remove

The design team felt that a tablet PC could accomplish the task of the first partition. A touch-screen display and stylus could be used as the primary user interface. The team decided on a Lenovo X61 tablet PC because of its proven design and cost. Additionally, accessories were available that would assist in protecting the device in arduous environments like those found aboard ship.

Figure 5-8: Lenovo X61 Tablet PC and Tablet Carrying Sleeve (http://www.lenovo.com)

To protect the tablet, the team decided on modifying a case similar to the one pictured to the right in Fig. 5-8. The PC is secured inside the sleeve with Velcro flaps that can protect the unit from minor debris and indirect water spray. The clamping mechanism used to secure the straps were very durable so the team decided to simply remove these from the straps and bolt them to standard mounting brackets typically used to secure light equipment to engineering bulkheads. This tablet / PC sleeve combination met the fulfilled the requirements of the COTS partition.

5.3.2 *New NEMA Enclosure*

The most significant changes suggested by the DSM involved the NEMA enclosure. The advances in COTS hardware and need for increased capability drove some major changes in the NEMA enclosure. The vision for the second generation NILM included the ability to use streaming data for near real time diagnostics. It needed to be easier to install and initialize than past systems for commercial appeal. The resulting needs of the NEMA Enclosure were:

- Minimal footprint
- Ability to stream up to six channels of data
- Simplification of transducer scaling resistor sizing
- Ethernet ready
- Ability to power itself off typical marine 440V system

The result was the new second generation NILM NEMA enclosure pictured in Fig. 5-9.
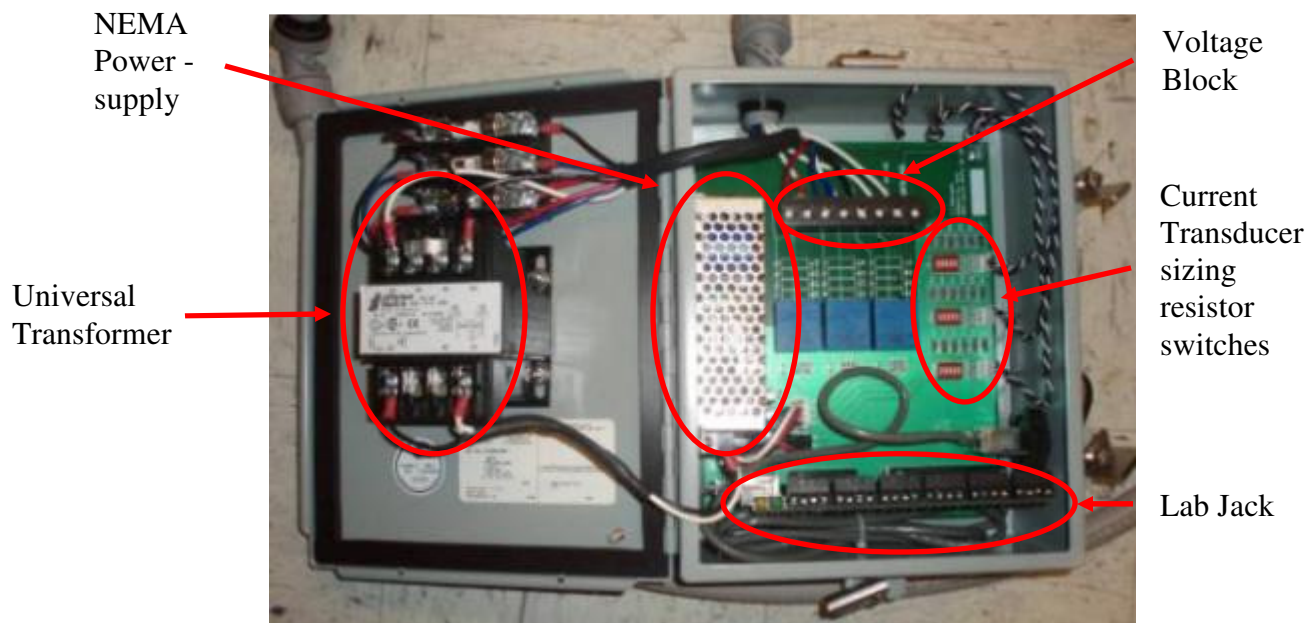

Figure 5-9: Second Generation NILM NEMA Enclosure

The universal transformer can be configured to step 208 – 480 Volts down to a 100 – 125 Voltage range that can be used by the NEMA power supply. The new enclosure can support monitoring of both delta and Wye configurations.

In the past, current transducer resistor sizing was very tedious. A power meter was used to determine a range of current the system to be monitored drew from the load center. Then a calculation was made to determine the sizing resistors that were to be installed across the terminal block in Fig. 5-1. With these sizing resistors organized in a DIP (Dual-Inline Package), an installer can quickly select a safe value, run an initial test and immediately set the current transducer sizing resistors. The new software developed by LCDR Ethan Proper and PhD candidate Jim Parish can scale both current and voltage transducers.

One significant detail that fell out of the DSM was that the Analog to Digital (A / D) converter should be moved outside the PC. The team began looking for a device that could be installed into the NEMA enclosure. Additionally, a high data-rate or one that could perform the A / D

Figure 5-10: Lab Jack Model UE9

function at a rate of at least 48kbits / second was desired (six channels sampled at a rate of 8kbits / second) to make streaming data possible. The Lab Jack UE9, USB/Ethernet based multifunction data acquisition and control device shown in Fig.5-10 was chosen to handle the A / D function. While this product seems more complex than needed, it enables data streaming. This made near real time interactive diagnostics possible.

5.3.3 *Target System*

The target system or system to be monitored will now also supply power to most of the NILM equipment. Voltage connections and current transducer installation will generally be done the same as with the first generation NILM. One change involves configuring the voltage block seen in Fig. 5-9 to support host system power. Two basic issues must be considered with respect to the voltage block. The first is whether a neutral is used (single phase or Wye configurations) and the second is choosing the phase of host power to be used.

5.4 Completed Installation

The new NILM hardware and software was developed and tested in LEES laboratory using a simple motor and dynamometer setup. Once the team was comfortable with the second generation NILM, it was installed aboard ship. The installation in Fig. 5-3 was removed and the second generation NILM installed. Figure 5-11 was taken aboard Escanaba shortly after installation and testing. Note how much cleaner the installation looks.

5-11: Second Generation NILM Install aboard CGC ESCANABA

5.4.1 *General Installation*

Installation of a second generation NILM set is quite different from its predecessor and less complicated for the most part. However, because of the additional capabilities of the new system, target system operational understanding becomes more essential. The NILM's impact on the system must be taken into account. This section is not meant to be a complete installation guide but is meant to provide a general outline for installation.

5.4.1.1 *Survey Target System Electrical interface.*

The first step to installing a NILM system on a particular piece of equipment is to obtain the load panel electrical line drawings. This is important for a number of reasons. The first of which is to locate a position downstream of the last possible protection device. Figure 5-12 is the inside of the CHT load panel after NILM install. The area circled in red represents the best place sample voltage and install current transducers.
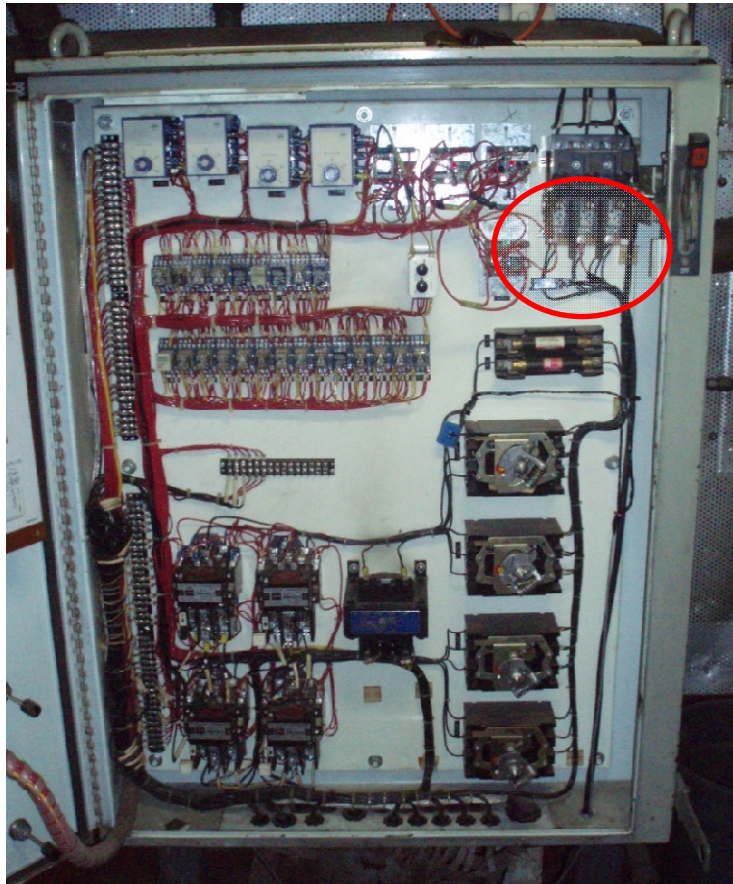
Figure 5-12: Open CHT Load Panel

A power meter should be used during the survey process to observe a complete operational cycle and maximum observed current noted. LEM current transducers (CTs) use model numbers like LA-150P, the numerical value in the model number is the maximum current

the CT is designed to operate with. Once the proper CT(s) is chosen, the target system must be studied to determine the optimal phase(s) to monitor. The equipment line diagram will come in handy here as well. For example Fig. 5-13 presents a power reading taken on phase A with the system in standby. Note that phase A shows a 200 Watt load. In some systems, 200 Watts is enough to cause a software diagnostic package hardship.

5-13: Auxiliary Load on CHT System Phase A

In the case of the CHT system, the best channel to monitor would be phase C. The next thing to consider is how best to access the load panel. Ships usually do not want extra holes drilled in equipment enclosures unless absolutely necessary. Any installation must maintain the integrity of the enclosure. Meaning, accesses must be semi-water tight.
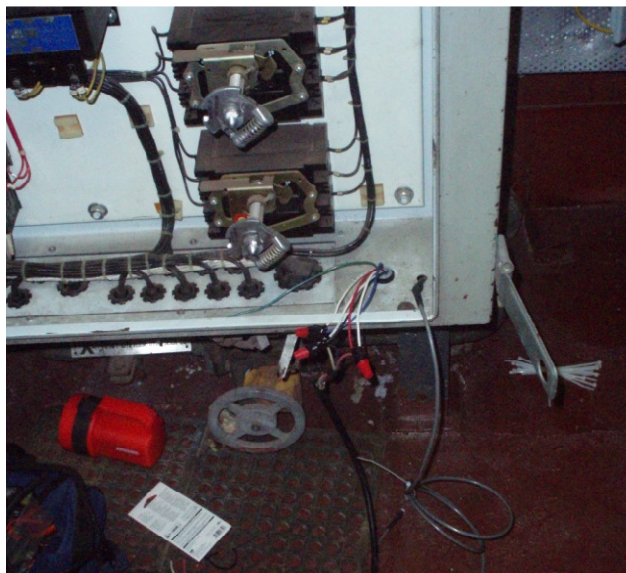
Figure 5-14: Accessing the Load Center

Once the CT and voltage connections have been made and properly passed through the target system enclosure, the NILM voltage block must be configured depending on the type of voltage sampled. NILM boxes are manufactured three phase Wye ready. However, most ships are three phase delta. The best place to make a delta to Wye conversion is at the voltage block circled in red.
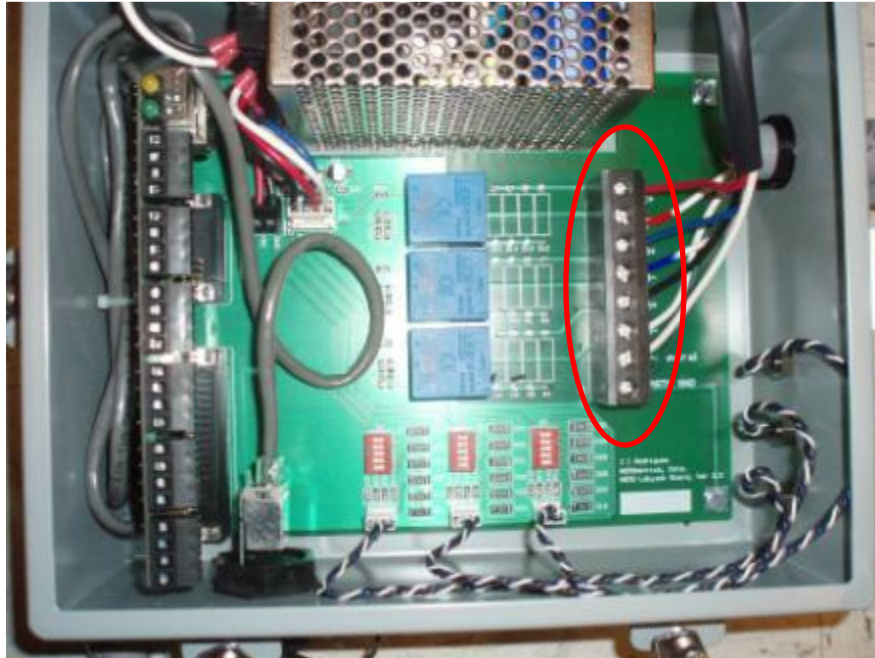
Figure 5-15: Second Generation NEMA Voltage Terminal Block

Mount the Computer in a location out of the way at eye level. It is usually best to survey the system end users to determine best placement. The NILM NEMA enclosure should be mounted as close to the load center as possible in a manner not to interfere with surrounding equipment and at least 12 inches off the deck.
.

5.5 Conclusions

As NILM moves forward, it is important for it to evolve into a system that can support a wider customer base and yet maintain the flexibility for employment in both shipboard and shore based applications. The new NILM architecture offers an incredible leap in capability and value to customers. The architecture should be revisited every two years to incorporate the benefits of new COTS technology as well as host ship systems.

6 Conclusions and Recommendations

6.1 Single Machine Monitoring

NILM has shown the ability to monitor a single induction machine using current harmonic quantities. However, there are both equipment orientation and physical design characteristics that can enhance this process. It was found that a simply loaded machine is more easily monitored in a horizontal direction vise a vertical one. Machine loading can potentially dampen the spectral quantities as well. These are considerations when monitoring both single machines and aggregate load centers.

A single machine diagnostic package should be developed. A suggested architecture for such a system is presented in Chapter 3. The basic physical building blocks for such a diagnostic system would be very similar to the ones presented in Chapter 5. A simple system or induction machine should be used to initially test the system.

6.2 Multiple Machine Monitoring

NILM has the ability to monitor multiple induction machines using an aggregate sensor. The test outlined in chapter 4 of this thesis should be replicated using two induction machines with differing key parameters and increased complexity. A system like the automated variable speed drive main engineroom ventilation system used aboard the Marine Protector Class Cutter should be investigated. This would present the NILM with a two induction machines and solid state variable speed drive.

6.3 Second Generation NILM Architecture

The architecture presented in this thesis was made possible primarily because of COTS hardware affordability. Five years ago the team would not have felt it was economically feasible to put a touch screen tablet PC on a Military vessel. Additionally, new product architectures like the Lab Jack (UE9) multifunction data acquisition and control module that enabled near real time data streaming as well as analog to digital functions. The current architecture should be reviewed in the next two years to take advantage of affordable technologies as well as ship technology advancements. For example, the ability to remotely transmit diagnostic information should be investigated.

List of References

[1]. Christopher Laughman, Kwangduk Lee, Robert Cox, Steven Shaw, Steven Leeb, Les Norford and Pete Armstrong, "Power Signature Analysis," IEEE Power & Energy Magazine, Vol. 1, Isue 2, pp. 56-63, March-April, 2003.

[2]. Cox, R,. M. Piber, G. Mitchell, P. Bennett, J. Paris, W. Wichakool, S. Leeb, 2007. *Improving Shipboard Maintenance Practices Using Non-Intrusive Load Monitoring.* In *Proc. of ASNE Intelligent Ships Symposium VII*, Philadelphia, PA, May 2007.

[3] Shaw, S. 2000. System identification techniques and modeling for non-intrusive load diagnostics. Ph.D. diss., Massachusetts Institute of Technology, Cambridge.

[4] Shaw, S., C. Abler, R. Lepard, D. Luo, S. Leeb, and L. Norford. 1998. Instrumentation for high performance nonintrusive electrical load monitoring. *ASME Journal of Solar Energy Engineering* 120: 224-229.

[5] Oppenheim, A., A. Willsky, and I. Young. 1988. *Signals and Systems.* Englewood Cliffs, NJ: Addison Wellesley

[6] Leeb, S., S. Shaw, and J. Kirtley. 1995. Transient event detection in spectral envelope estimates for nonintrusive load monitoring. *IEEE Trans. on Power Delivery* 10: 1200–1210.

[7] Lee, K. 2003. Electric load information system based on non-intrusive power monitoring. Ph.D. diss., Massachusetts Institute of Technology, Cambridge.

[8] Cox, R., J. Mosman, T. McKay, S. Leeb, and T. McCoy. 2006. Diagnostic indicators for shipboard cycling systems using non-intrusive load monitoring. In *Proc. ASNE Day 2006*, June, Arlington, VA.

[9] Cox, R. 2006. Minimally intrusive strategies for fault detection and energy monitoring. Ph.D. diss., Massachusetts Institute of Technology, Cambridge.

[10] Laughman, C., P. Armstrong, L. Norford, and S. Leeb, 2006. The detection of liquid slugging phenomena in reciprocating compressors via power measurements. In *Proc. International Compressor Engineering Conference at Purdue*, July, West Lafayette, IN.

[11] DeNucci, T. et al. 2005. Diagnostic indicators for shipboard systems using non-intrusive load monitoring. In *Proc. 1st IEEE Electric Ship Technologies Symposium*, July, Philadelphia, PA.

[12] Mitchell, G., R. Cox, J. Paris, and S. Leeb. 2007. Shipboard fluid system diagnostic indicators using non-intrusive load monitoring. To appear in *Proc. ASNE Day 2007*, June, Arlington, VA.

[13]   Cox, R., P. Bennett, T. McKay, J. Paris, and S. Leeb. 2007. Using the non-intrusive load monitor for shipboard supervisory control.   To appear in *Proc. 2nd IEEE Electric Ship Technologies Symposium*, May, Arlington, VA.

[14]   Paris, J. 2006. A framework for non-intrusive load monitoring and diagnostics. M.Eng. thesis, Massachusetts Institute of Technology, Cambridge.

[15]   McKinnon, David, Bethe, Noah,'Fault Done Analysis: Identifying Motor Defects Using the Rotor Fault Zone," IEEE Power and Industry Conf., 2005 pp 400-407.

[16]   Jason Stack, Thomas Habetler, Ronald Harley, "Bearing Fault Detection via Autoregressive Stator Current Modeling," IEEE Transactions on Industry Applications, Vol. 40, No. 3, May/June 2004.

[17]   J.S. Ramsey, Jr. "Shipboard Applications of Non-Intrusive Load Monitoring", Massachusetts Institute of Technology NSEE/S.M. EECS thesis, June 2004.

[18]   R. R. Schoen and T. G. Habetler, "Motor bearing Damage Detection Using stator current monitoring,"IEEE Trans. on Ind. Applic., vol. 31, no. 6, Dec 1995. pp 1274 – 1279.

[19]   A. Oppenheim, R. S. (1999). *Discrete-Time Signal Processing.* New Jersey: Prentice Hall.

[20]   Signals and Systems by Oppenheim and Willsky

[21]   LEM Corporation, Current and Voltage Transducers for Industrial Applications

[22]   Bennett, P. "Using the Non-Intrusive Load Monitor for Shipboard Supervisory Control," Massachusetts Institute of Technology S.M thesis June 2007.

[23]   Proper, E. 2008. Automated Classification of Power Signals. M.Eng. thesis, Massachusetts Institute of Technology, Cambridge.

[24]   K. Hurst, T Habetler, "Sensorless Speed Measurement Using Current Harmonic Spectral Estimation in Induction Machine Drives," IEEE Trans. On Power Elect., vol.11, no. 1, Jan 1996. pp 66 – 73.

[25]   IAS Motor Reliability Working Group, "Report of large motor reliability survey of industrial and commercial installations:, Part I," IEEE Trans. Ind. Applicat., vol.IA-21, no. 4, pp 853-864, July 1985.

[26]   R.R. Schoen and T.G. Habetler, "Effects of Time-Varying Loads on Rotor Fault Detection in Induction Machines." IEEE Transactions on Industry Applications, Vol. 31, pp. 900-906, July/Aug 1995.

[27]   DLI Watchman ST-101 Vibration Screening Tool Online Operator's Guide. http://www.spintelligentlabs.com/SL-docs/st-101-og-flat.pdf 15 May 2007

[28]   G. B. Kilman and J. Stein, "Induction motor fault detection via passive current monitoring," in Proc. Int. Conf. E.ec. Mach., Aug 1990, pp. 13-17.

[29]   R. R. Schoen and T. G. Habetler, "Effects of time-varying loads on rotor fault detection in induction machines," in Conf. Rec. 28th annu. IAS Meeting, Oct. 1993, pp. 324-330.

[30]   J. Brandlein, et.al., Ball and Roller Bearings: Theory, Design and Application. Chichester: John Wiley & Sons, 1999.

[31]   T.A. Harris and M.N. Kotzalas, Advanced Concepts of Bearing Technology. CRC Press, 2007.

[32]   Buffalo, N.(2008). DSM Tutorial. Retrieved January 21, 2008, from Design Structure Matrix (DSM) Homepage: http://www.dsmweb.org/